



ARL-TR-7860 • OCT 2016



Design and Calibration of the US Army Research Laboratory (ARL) Closed Loop Laboratory Radio Frequency (RF) Propagation Section

by William Coburn, Seth A McCormick, and Andre F Witcher

NOTICES

Disclaimers

The findings in this report are not to be construed as an official Department of the Army position unless so designated by other authorized documents.

Citation of manufacturer's or trade names does not constitute an official endorsement or approval of the use thereof.

Destroy this report when it is no longer needed. Do not return it to the originator.



Design and Calibration of the US Army Research Laboratory (ARL) Closed Loop Laboratory Radio Frequency (RF) Propagation Section

by William Coburn, Seth A McCormick, and Andre F Witcher
Sensors and Electron Devices Directorate, ARL

REPORT DOCUMENTATION PAGE			Form Approved OMB No. 0704-0188		
<p>Public reporting burden for this collection of information is estimated to average 1 hour per response, including the time for reviewing instructions, searching existing data sources, gathering and maintaining the data needed, and completing and reviewing the collection information. Send comments regarding this burden estimate or any other aspect of this collection of information, including suggestions for reducing the burden, to Department of Defense, Washington Headquarters Services, Directorate for Information Operations and Reports (0704-0188), 1215 Jefferson Davis Highway, Suite 1204, Arlington, VA 22202-4302. Respondents should be aware that notwithstanding any other provision of law, no person shall be subject to any penalty for failing to comply with a collection of information if it does not display a currently valid OMB control number.</p> <p>PLEASE DO NOT RETURN YOUR FORM TO THE ABOVE ADDRESS.</p>					
1. REPORT DATE (DD-MM-YYYY) October 2016		2. REPORT TYPE Technical Report		3. DATES COVERED (From - To) 08/2016	
4. TITLE AND SUBTITLE Design and Calibration of the US Army Research Laboratory (ARL) Closed Loop Laboratory Radio Frequency (RF) Propagation Section			5a. CONTRACT NUMBER		
			5b. GRANT NUMBER		
			5c. PROGRAM ELEMENT NUMBER		
6. AUTHOR(S) William Coburn, Seth A McCormick, and Andre F Witcher			5d. PROJECT NUMBER R.0018631.2		
			5e. TASK NUMBER		
			5f. WORK UNIT NUMBER		
7. PERFORMING ORGANIZATION NAME(S) AND ADDRESS(ES) US Army Research Laboratory ATTN: RDRL-SER-M 2800 Powder Mill Road Adelphi, MD 20783-1138			8. PERFORMING ORGANIZATION REPORT NUMBER ARL-TR-7860		
9. SPONSORING/MONITORING AGENCY NAME(S) AND ADDRESS(ES)			10. SPONSOR/MONITOR'S ACRONYM(S)		
			11. SPONSOR/MONITOR'S REPORT NUMBER(S)		
12. DISTRIBUTION/AVAILABILITY STATEMENT Approved for public release; distribution is unlimited.					
13. SUPPLEMENTARY NOTES					
14. ABSTRACT <p>The Closed Loop Laboratory includes a radio frequency (RF) propagation section from 8–18 GHz using broadband dual-ridged horn antennas (DRHAs) in an absorber-lined chamber. The aluminum chamber is constructed in 2 halves, 4 ft (W) × 4 ft (H) × 4 ft (L) connected by clamps so it can be opened as needed. Three DRHAs are mounted on each end of the 8-ft-long chamber on metal shafts oriented in a triangle pattern with independent rotation control. The entire 3-horn assembly on each end of the chamber is installed with clamps so that they can be removed. All the cables/connectors used to connect the network analyzer to the propagation section inputs are calibrated out of the measurements. However, the short cables between the input to the chamber and the horn input are not included, so their insertion loss is measured separately and the data corrected for this additional loss. Measurements are conducted from 7–19 GHz, where the measured transmission and coupling data represent the calibration of the entire RF propagation section. Calculated path loss and numerical simulations are shown to demonstrate that the chamber performance can be approximated by free space calculations or numerical simulations of the horn configuration.</p>					
15. SUBJECT TERMS FEKO, Closed Loop Laboratory, radar, horn antenna, transmission, coupling					
16. SECURITY CLASSIFICATION OF:			17. LIMITATION OF ABSTRACT UU	18. NUMBER OF PAGES 50	19a. NAME OF RESPONSIBLE PERSON William Coburn
a. REPORT Unclassified	b. ABSTRACT Unclassified	c. THIS PAGE Unclassified			19b. TELEPHONE NUMBER (Include area code) 301-394-2705

Contents

List of Figures	iv
List of Tables	v
Acknowledgments	vi
1. Introduction	1
2. CLL RF Section Description	3
3. RF Propagation Chamber Setup and Calibration	8
4. RF Section Modeling	10
5. RF Section Measurements	20
6. Conclusions	32
7. References	33
Appendix. Equipment Used	35
List of Symbols, Abbreviations, and Acronyms	41
Distribution List	42

List of Figures

Fig. 1	CLL system block diagram.....	1
Fig. 2	Radar simulator configuration	2
Fig. 3	Aluminum RF section showing clamps available for opening the chamber.....	4
Fig. 4	Tapered resistivity 4.5-inch metal-backed microwave absorber reflectivity data (image courtesy of MAST Technologies ²)	4
Fig. 5	DRHA specifications (image courtesy of A-INFO ³)	5
Fig. 6	Manufacturer's measured gain vs. frequency for DRHA numbers 101 and 102.....	5
Fig. 7	DRHAs on rotating shafts from a) inside, b) outside, and c) removed..	6
Fig. 8	Scale drawing of a) the absorber-lined propagation chamber and b) the DRHA arrangement on a 4-inch base (and height) triangle	7
Fig. 9	Initial calibration setup and configuration	8
Fig. 10	Propagation chamber setup and configuration.....	9
Fig. 11	The free space realized gain of a DRHA for a) the FEKO horn model compared to a single A-INFO horn and b) the FEKO horn compared to a 6-horn model	12
Fig. 12	The free space realized gain E-plane pattern at 12 GHz for DRHAs a) using the FEKO single-horn model compared to 3 horns, b) a single horn compared to the 6-horn model, c) the corresponding cross-polarized component with and without symmetry, and d) the rotated TX horn cross-polarized pattern	15
Fig. 13	The simulated S-parameters for ridge horn antennas for a) a 3-horn model and b) a 6-horn model	17
Fig. 14	The free space PL for SGH antennas a) from FEKO compared to the calculated PL and b) the difference vs. frequency	19
Fig. 15	The free space PL for 2 DRHAs from theory using the measured gain vs. frequency, the typical gain, and from a FEKO simulation.....	20
Fig. 16	The measured horn 1 reflection coefficient vs. frequency compared to the FEKO models.....	21
Fig. 17	The measured horn reflection coefficients vs. frequency	21
Fig. 18	The measured insertion loss for a short cable penetrating the CLL for connecting the horns	22
Fig. 19	The measured co-polarized horn coupling vs. frequency compared to the FEKO model	23
Fig. 20	The measured co-polarized horn coupling vs. frequency compared to the VNA noise level.....	24

Fig. 21	The measured transmission for co-polarized horns vs. frequency without correction	25
Fig. 22	The corrected data for transmission of co-polarized aligned horns vs. frequency.....	25
Fig. 23	The corrected data for transmission and coupling of a cross-polarized TX horn vs. frequency	26
Fig. 24	The measurement summary for a) the dynamic range for co-polarized transmission based on noise level, b) the cross-polarized transmission and noise level, and c) the noise level for reception based on nearest neighbor coupling	27
Fig. 25	The measured data without correction for transmission of co-polarized horns compared to calculated and simulated PL.....	28
Fig. 26	The corrected data for transmission of co-polarized horns vs. frequency.....	29
Fig. 27	The corrected co-polarized data summary compared to calculated/simulated results vs. frequency.....	30
Fig. 28	The corrected a) co-polarized and b) cross-polarized data summary compared to FEKO simulated results vs. frequency.....	31
Fig. A-1	Electronic calibration module calibration certificate	37
Fig. A-2	Network analyzer calibration certificate	38
Fig. A-3	Foam absorber data sheet.....	39
Fig. A-4	A-INFO horn typical gain vs. frequency (image courtesy of A-INFO).....	40
Fig. A-5	A-INFO horn typical cross-polarized response vs. frequency (image courtesy of A-INFO ²)	40

List of Tables

Table A-1	Equipment and parts list.....	36
-----------	-------------------------------	----

Acknowledgments

We would like to acknowledge Timothy Burcham for the mechanical design and construction of the radio frequency propagation section and horn mounting arrangement. We also acknowledge the efforts of Timothy Burcham and Arthur Harrison for the installation of this chamber in the Closed Loop Laboratory. Finally, we acknowledge Neal Tesny for creating and calibrating the rotation control software.

1. Introduction

The objective for the design and development of a radio frequency (RF) Closed Loop Laboratory (CLL) is to develop a capability to emulate the phenomenology, waveform, and modulation techniques of Army RF systems and other national assets. It also is being developed to gain a better understanding of current system limitations and will aid in the development of techniques, waveforms, and algorithms for improved system performance. This design provides the US Army Research Laboratory (ARL) with a unique facility for the study of current and evolving RF systems. The CLL is a closed loop simulator that can be used to model, simulate, and analyze the effects and phenomenology for both simulated and actual RF transmissions and receiver signature profiles to include, but not limited to, radar and communications systems.

The CLL comprises 3 major assemblies: the RF transmitter simulator, the RF propagation section, and the target generator to mimic the analog composition of the radar target return and impose other environmental effects such as radar cross section (RCS) profiles and micro-Doppler stimuli. Figure 1 shows a block diagram of these assemblies, configured as a radar emulator for the purposes of this report, which focuses on the design and calibration of the RF propagation section. The CLL is designed to also simulate, as close as possible, the environmental effects that a radar-generated signal and its return may experience as part of an impact study. The effects include, but are not limited to, electric-field (E-field) polarization, atmospheric conditions, and range effects.

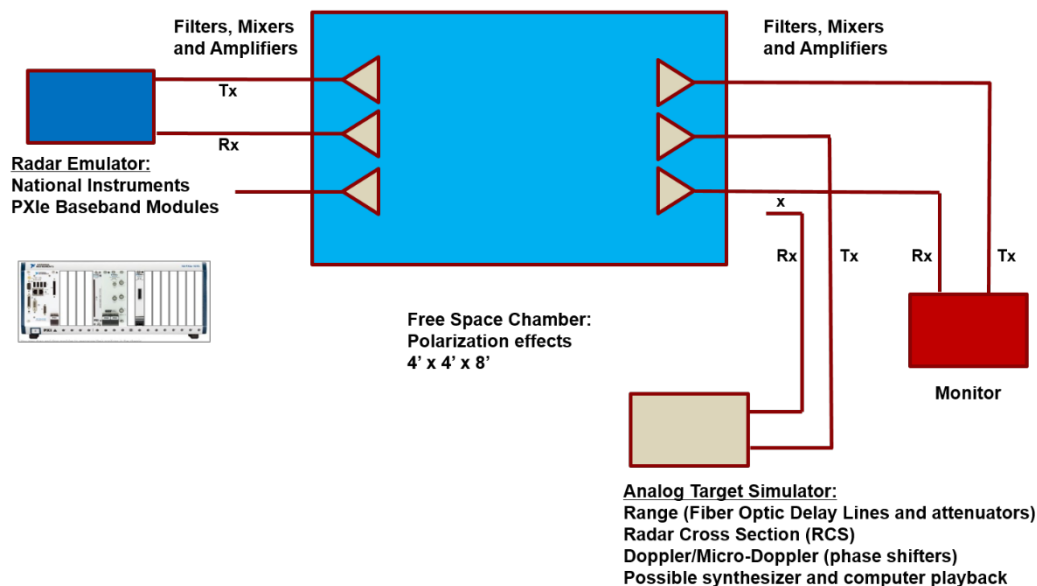


Fig. 1 CLL system block diagram

The design philosophy for the RF CLL was to use a modular design approach, which would allow for system expansion and growth to accommodate mission needs and address evolving waveforms that would require upgrades to the system. The radar simulator comprises a National Instruments (NI) 18-slot Peripheral Component Interconnect Extensions for Instrumentation Express (PXIe) chassis populated with various modules used for waveform generation and process control.¹ The system is designed to allow for direct insertion of radar profiles by the operators so that a visual response and reaction can be ascertained and analyzed. Figure 2 shows the chassis that contains the PXIe-1085 that makes up the radar simulator. It is configured, at a minimum, with a system controller, a PXIe-8135, a digitizer/analog-to-digital converter (PXIe-5154), a digital-to-analog converter, and a 500-GB SATA hard drive for mass storage. Future upgrades might include the NI PXIe-7965R Flex Rio field-programmable gate array module. The chassis could be used to accommodate a programmable step attenuator used to emulate environmental conditions. The free space test chamber will mimic wave propagation effects. It will include polarization studies and effects as selected antenna are positioned in predefined orientations, from either a radar emitter perspective or a target perspective.

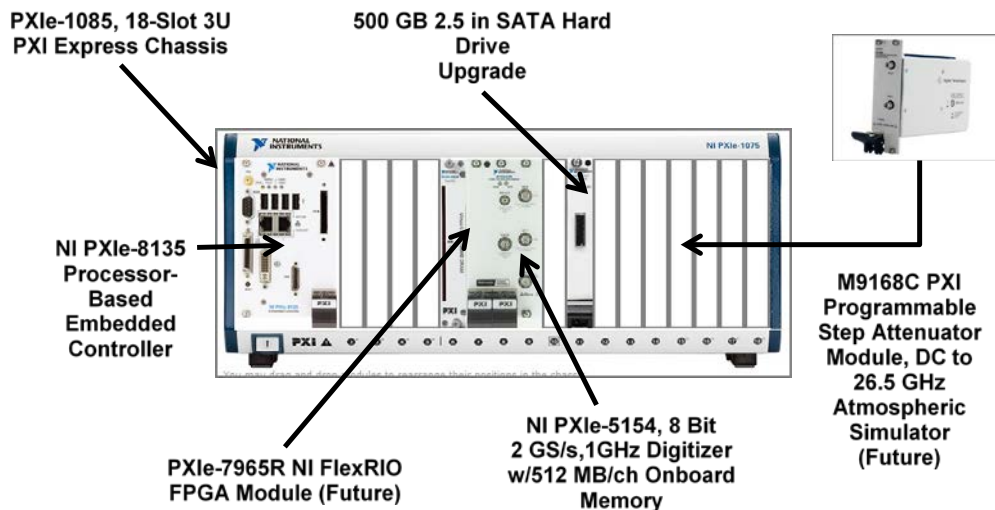


Fig. 2 Radar simulator configuration

The overall CLL system configuration consists of a network of RF cabling assemblies, mixers, directional couplers, and power conversion devices. These are connected to produce the proper radar and target generator transmit (TX) and receive (RX) functions and capabilities, as well as a methodology for capturing the closed loop response in real time as described by the NI instrumentation. The radar transmits/radiates its baseband derived waveforms, which is further mixed up or down depending on the requirement into the free space chamber to emulate as close

as possible prevailing atmospheric conditions (rain, snow, fog, etc.). Once the propagated radar wave exits the chamber, it is directed through couplers or power splitters to the target simulator where it is further scrutinized by the target generator and retransmitted back into the test chamber where it is received and processed to measure the effects.

2. CLL RF Section Description

The CLL includes an RF propagation section from 8–18 GHz using broadband dual-ridged horn antennas (DRHAs) in an absorber-lined chamber. The aluminum chamber is constructed in 2 halves, 4 ft (W) \times 4 ft (H) \times 4 ft (L), connected by clamps so it can be opened as needed as shown in Fig. 3. The tapered resistivity absorber is a MF-51 from MAST Technologies, which has better than -35 dB reflectivity over the frequency range of interest.² The manufacturer's measured reflectivity for this 4.5-inch-thick foam absorber is shown in Fig. 4, with the data sheet included in the Appendix, although this product is no longer available. The DRHAs were obtained from A-INFO, Inc., and meet the manufacturer's specifications shown in Fig. 5.³ Compact horn antennas are used since gain is less important than maintaining a portable size chamber. Two of the measured gain curves provided with the horns were digitized and are compared in Fig. 6, indicating only small differences over the frequency band. Three of these horns are mounted on each end of a 4-ft (W) \times 4-ft (H) \times 8-ft (L) chamber on metal shafts oriented in a triangle pattern with independent rotation control as shown in Fig. 7 as installed in the absorber-lined chamber. The shaft motors are controlled independently using LabView.⁴ The horns are connected to the shafts using aluminum brackets to the existing bolts for the coax-to-waveguide adaptor (see Fig. 7). The entire assembly is installed with clamps so that it can be removed as shown in Fig. 7c. Because of this installation, there is a gap in the absorber lining around the horn assembly as can be seen in Fig. 7a. Notice that short Crystek cables from the chamber inputs penetrate the chamber through the shafts as can be seen in Fig. 7b.



Fig. 3 Aluminum RF section showing clamps available for opening the chamber

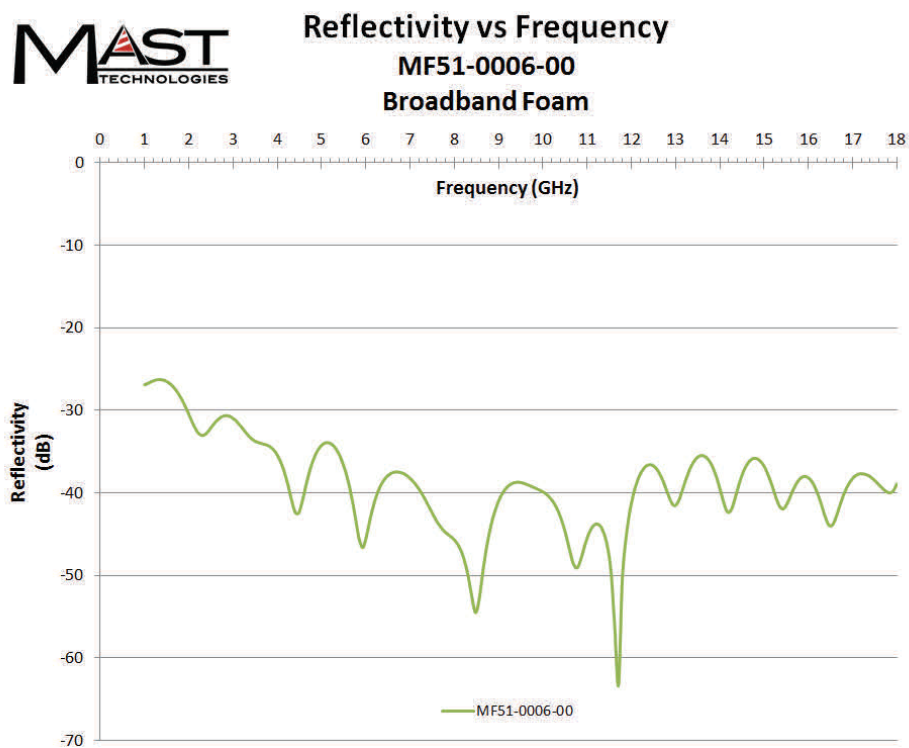


Fig. 4 Tapered resistivity 4.5-inch metal-backed microwave absorber reflectivity data (image courtesy of MAST Technologies²)

Approved for public release; distribution is unlimited.

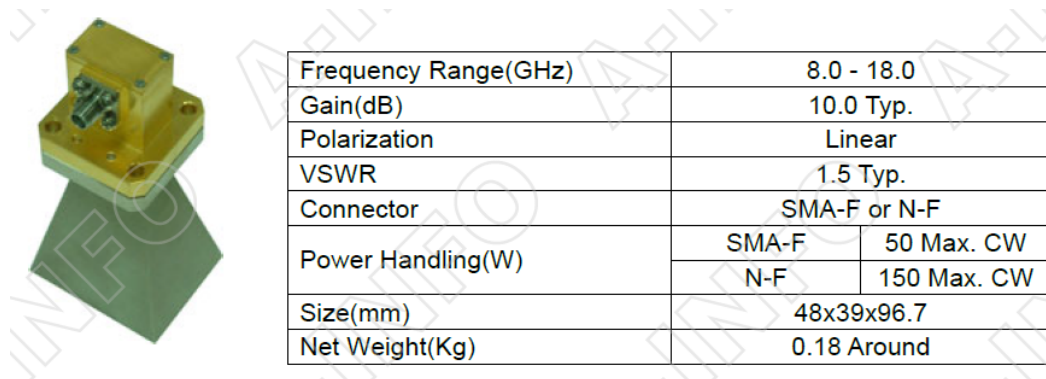


Fig. 5 DRHA specifications (image courtesy of A-INFO³)

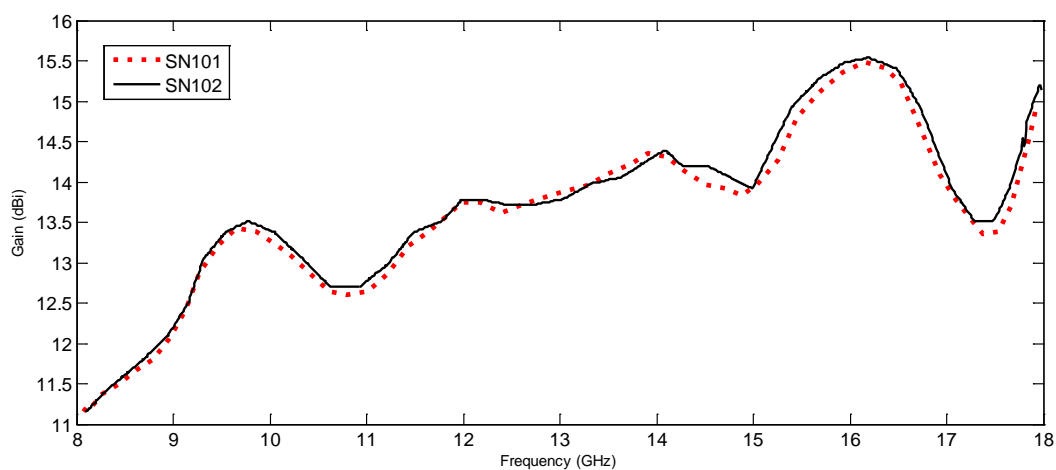
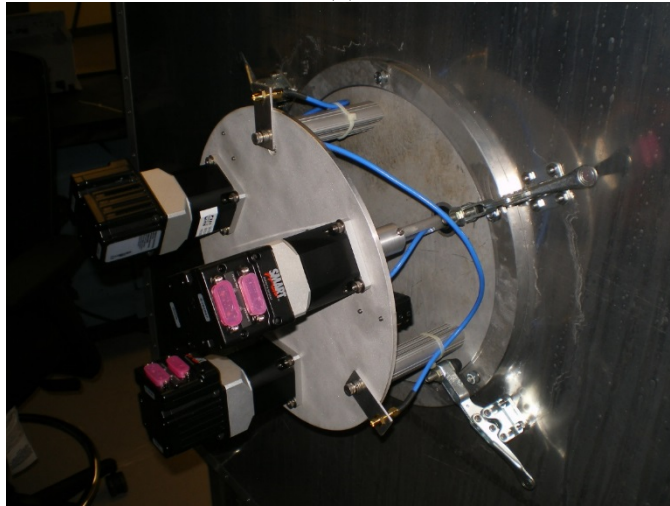


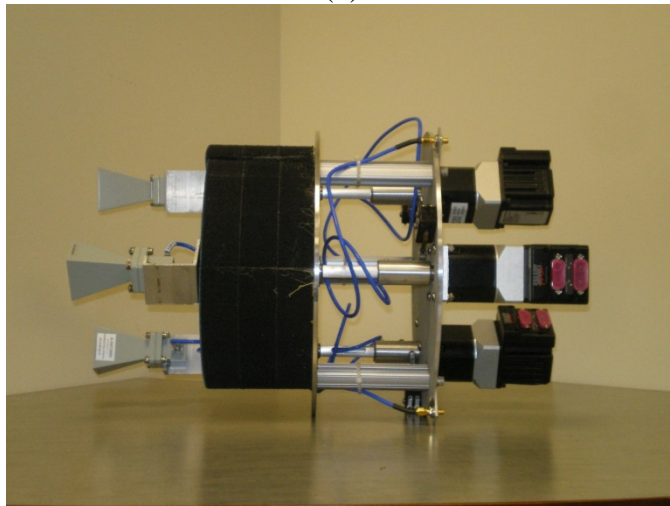
Fig. 6 Manufacturer's measured gain vs. frequency for DRHA numbers 101 and 102



(a)



(b)



(c)

Fig. 7 DRHAs on rotating shafts from a) inside, b) outside, and c) removed

A scale drawing is shown in Fig. 8 where the horn aperture is roughly 8.3 inches from the wall leaving a separation distance $d = 6.6$ ft. (2 m) between the horn apertures. A horn 8.3 inches from the center of the back wall would have a 52° field of view to the center of the chamber side walls. Based on the manufacturer's specifications, the full beam width is approximately 53° at 8.5 GHz decreasing to approximately 33° at 18 GHz. So at the lowest frequency the main beam of the radiation pattern would be about 3 dB lower at the side wall compared to the direct path. Thus, the reflection from the side walls should be more than 30 dB less than the main beam over the entire frequency range. However, empirical calibration is required to account for scattering effects not included in a theoretical or numerical analysis. It should be mentioned that the DRHA numerical model is somewhat idealized and the horn arrangement for simulations is perfectly symmetric around the vertical centerline (see Fig. 7b). This leads to some unrealistic results, especially when one horn is cross-polarized.

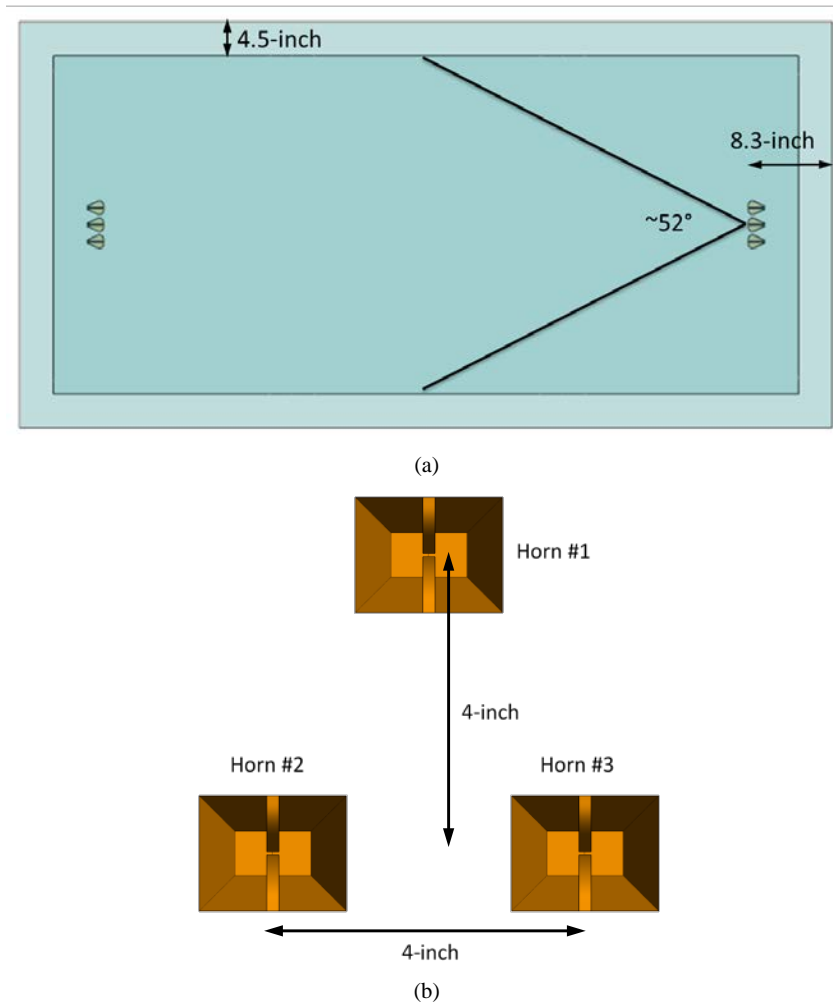


Fig. 8 Scale drawing of a) the absorber-lined propagation chamber and b) the DRHA arrangement on a 4-inch base (and height) triangle

The separation between horns must satisfy the far-field requirement. At the lowest frequency, the wavelength $\lambda_{\max} = 37.5$ mm, and $d \gg \lambda_{\max}$ implies a separation greater than 0.4 m. At the highest frequency, $d > 2D^2/\lambda_{\min}$, where $D = 61.8$ mm is the horn aperture diagonal and $\lambda_{\min} = 17$ mm so $d > 0.315$ m. The 2-m aperture separation satisfies both requirements. With an absorber reflectivity of greater than 30 dB, the chamber should be similar to free space conditions. Any deviations can be corrected with frequency-dependent calibration factors, but these corrections should be small. Free space path loss (PL) calculations and numerical simulations are used to estimate the various S-parameters. The chamber measured S-parameter data for cross-talk and PL over the aperture separation establish the actual calibrated levels. Then RF propagation effects such as polarization mismatch can be investigated. Other uses for such a chamber are material studies such as absorber transmission, the influence of radomes, and other scattering experiments.

3. RF Propagation Chamber Setup and Calibration

The initial setup and calibration for the propagation section is depicted in Fig. 9. Figure 10 depicts the setup used for the calibration of the chamber. The Keysight M9375A vector network analyzer (VNA) and Keysight N4691B Electronic Calibration (ECal) 2-port module were used to perform the initial calibration prior to connecting to the chamber. The ECal module is controlled by the USB interface to the NI PXIe-8135 system control module. In this manner, the cables used to connect the VNA to the chamber are included in the calibration so their insertion loss are not part of the measured chamber PL.

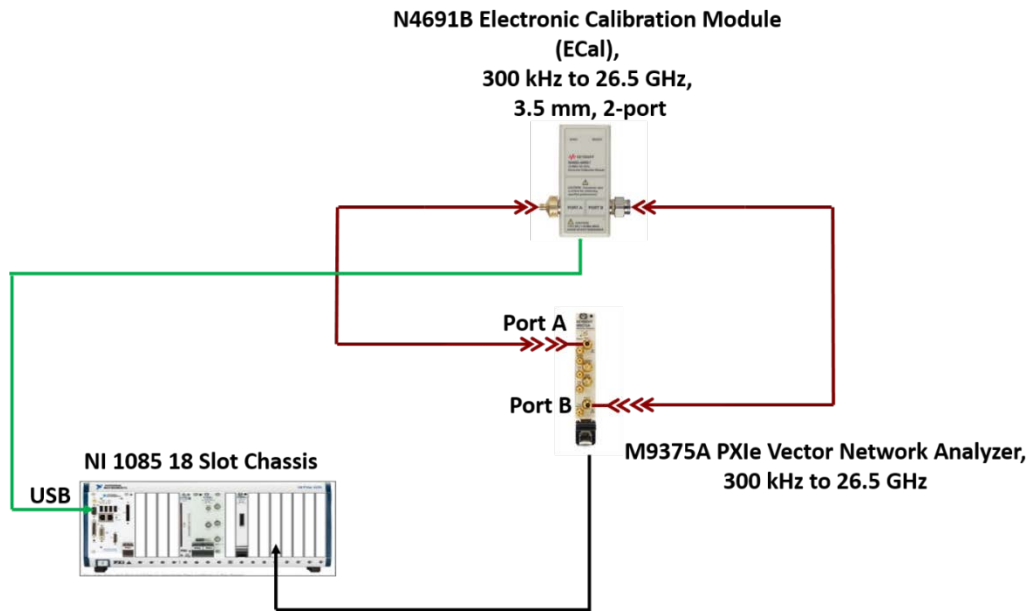


Fig. 9 Initial calibration setup and configuration

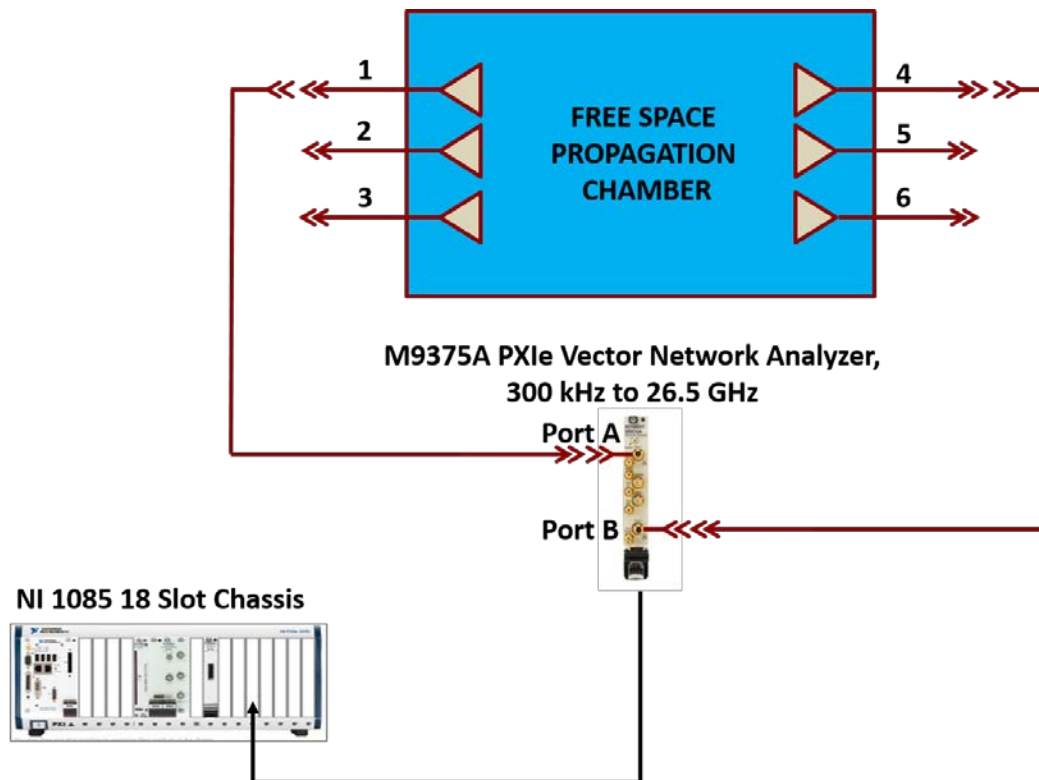


Fig. 10 Propagation chamber setup and configuration

The M9375A VNA module is housed in and occupies a slot in the NI 18-slot chassis. Keysight proprietary network analyzer software, when launched from within the Windows-based controller environment, is used to configure and initiate calibration of VNA prior to connecting the test cables to the chamber. The calibration employing the ECal module is used to account for and eliminate any losses and errors generated by the test cables, adapters, and VNA prior to performing any test on the free space propagation chamber. The ECal module is designed to automate the entire calibration process. The ECal module replaces the traditional network analyzer calibration processes where shorts, opens, and loads were physically inserted directly into the test setup prior to the test article, in this case, the chamber. Using the ECal module ensures confidence and repeatability into the test setup. Thus, minimizing the possibility of collecting erroneous data that would impact test results.

Cables are connected to the ECal modules Port A and B 3.5-mm male connectors using two 2-ft male to male extension cables, which are further connected to two 10-ft lengths of SMA male to male cables. The 2-ft lengths were inserted into the setup to relieve stress on the 3.5-mm straight input connectors of the M9375A VNA. These 2-ft cables are used for all subsequent measurements so the VNA calibration extends to the chamber inputs. All the cables being used to connect the

VNA to the propagation chamber are thus calibrated out of the measurements. However, the short cables between the input to the chamber and the horn input are not included in the calibration. The insertion loss of these cables is measured separately and the data corrected for this additional loss. That is, the measured transmission is smaller than the free space PL owing to the additional insertion loss of these cables, which can be corrected to obtain only the PL of the RF section.

Calibration and measurements are conducted over frequencies of 7–19 GHz and the horns are still matched over this frequency band. The intermodulation frequency (IF) bandwidth is set to 100 Hz with 10,000 frequency samples. After calibration is completed and saved, the ECal module is removed and the cables are connected to the chamber as shown in Fig. 10. Measurements such as S-parameters can be performed, saved, and analyzed. The specifications data provided for both the M9375A VNA and N4691B ECal modules are National Institute of Standards and Technology traceable through Keysight Technologies. The calibration certificate for both can be found in the Appendix.

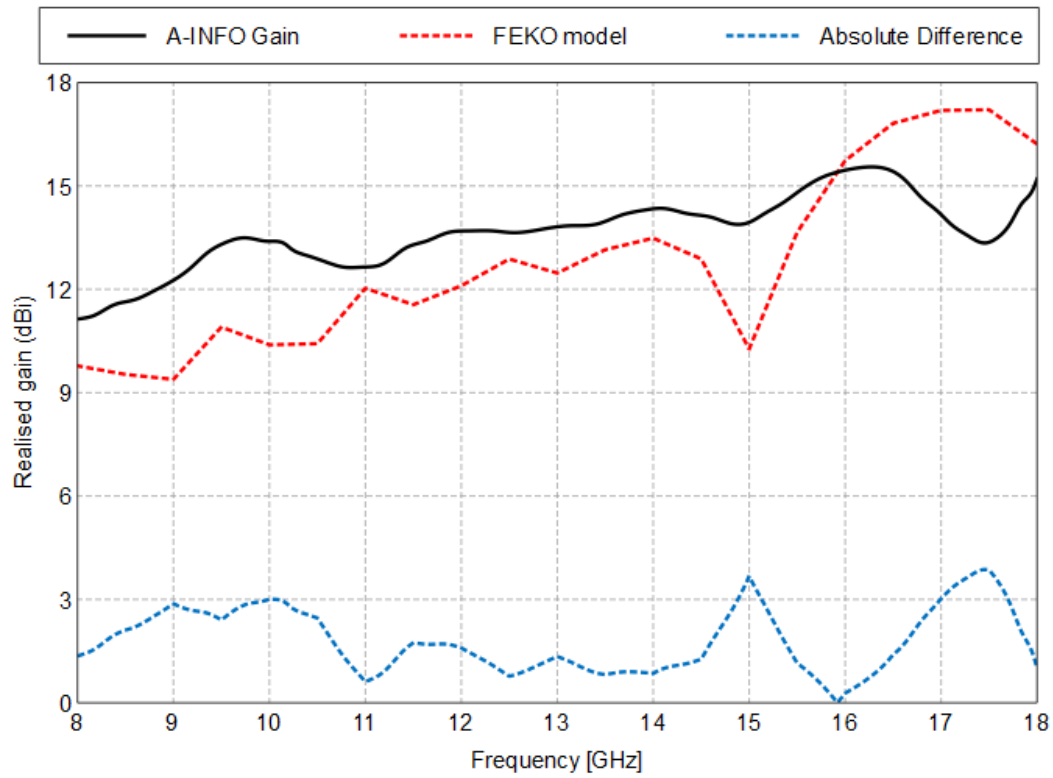
4. RF Section Modeling

To properly model the free space propagation, an accurate horn model was required, but an exact computer-aided design model of the A-INFO horns was not available. Instead, a dual-ridged horn from the antenna repository software Antenna Magus was chosen as an approximate model.⁵ The aperture size had to be scaled to the same aperture size as the A-INFO horns: 1.89 inches (48 mm) \times 1.54 inches (39 mm). The length of the model horn, however, is shorter by about 0.2 inches (5 mm). The horn model was simplified and the coax (waveguide port) was substituted with a magnetic frill source (edge port). FEKO, a commercial software suite for electromagnetic modeling, was the primary solver using the method of moments for small problems (1–4 horns) and the multi-level fast multipole method (MLFMM) for large (6 horns) problems.⁵ Three workstations in total were used for FEKO simulations. Two workstations had two 12-core, hyper-threaded Intel Xeon central processing units (CPUs) clocked at 3.1 GHz under load (2.3 GHz at idle), 128 GB of DDR4 random-access memory (RAM), and one NVidia Quadro K6000 graphics processing unit (GPU) each. The other workstation was a standalone Linux machine (CentOS GNOME) with four 16-core AMD Opteron CPUs clocked at 2.6 GHz under load (2.3 GHz at idle), 256 GB of DDR3 RAM, and one NVidia GTX 680 GPU. All stated computational times and memory requirements were calculated as the average per frequency.

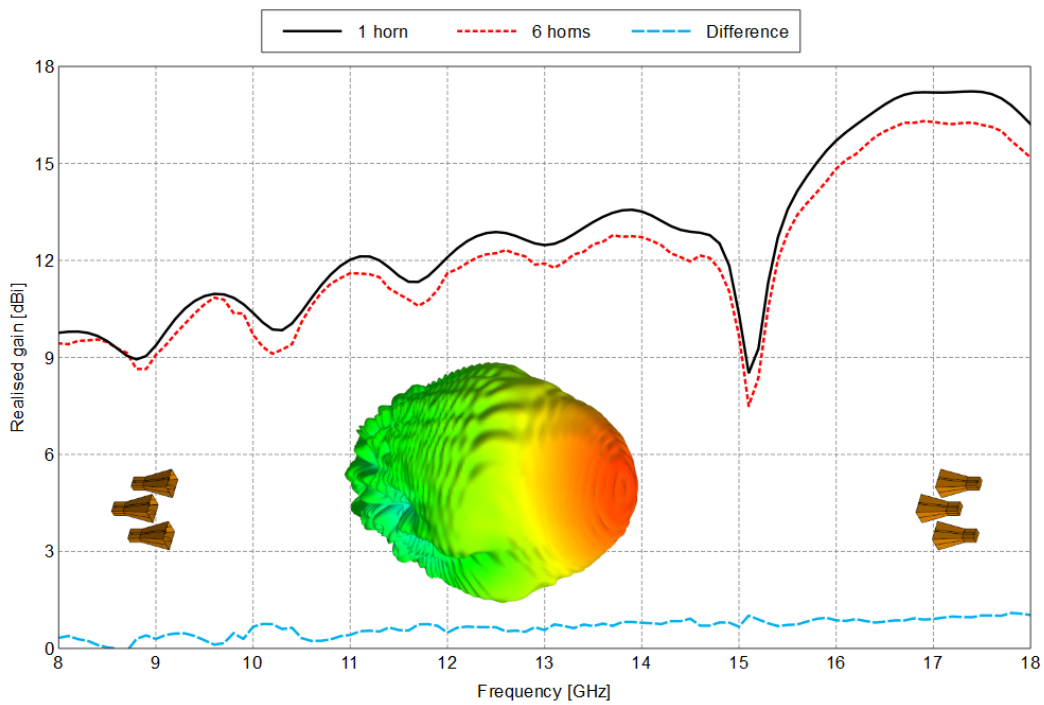
Magnetic symmetry is enforced in all co-polarized horn models for faster computations and reduction in memory usage for simulations without MLFMM.

Symmetry is still used for MLFFM simulations to enforce a symmetric mesh. Symmetry is not recommended for the cross-polarized model. The plane of symmetry forces the E-field to be perfectly symmetric beyond that of an idealized model, which produces perfect cross-polarization, which could never be achieved in practice. All shown patterns are in the plane of the E-field (E-plane). Co- and cross-polarized simulations refer to the polarization of the transmitting horn (horn 4 in the chamber). Co-polarized refers to the transmit horn being co-polarized with all other horns. Cross-polarized refers to the transmit horn being cross-polarized with respect to all other horns.

A comparison of the A-INFO and simulated horn gain is shown in Fig. 11a indicating the actual horns used have more gain at most frequencies. Above 16 GHz, the horn model has a higher gain than the A-INFO horns. The difference in the horn transition length is the most likely culprit for the gain difference. A frequency-dependent correction factor can be used to scale the FEKO model gain to that specified for the A-INFO horns so the model can more accurately represent the A-INFO horn configuration. Neglecting this difference in gain, the FEKO model is still useful for approximating the A-INFO horns in terms of S-parameters, radiation patterns, near-fields, and coupling. For a single horn using a 12-core CPU and one plane of symmetry, the FEKO simulation requires 0.94 GB of RAM and about 43 s per frequency for single precision. A 3-horn model for simulating the cross-talk to nearby horns requires 6.7 GB of RAM and about 302 s per frequency for single precision. Neither the single- nor 3-horn models used MLFFM, as the problem space was too small electrically for this method to save computational resources.



(a)



(b)

Fig. 11 The free space realised gain of a DRHA for a) the FEKO horn model compared to a single A-INFO horn and b) the FEKO horn compared to a 6-horn model

Part of the purpose of the modeling exercise was to determine how simple a model could be used to approximate RF propagation in the CLL. The reason being that a simple model reduces computational resources and time at the expense of accuracy. For example, modeling 3 nearby horns to simulate coupling (or cross-talk) or even 4 horns for transmission and coupling would be preferred instead of 6 horns. Comparing the gain and radiation pattern of 1 horn to 6 horns is a good way of capturing perturbations caused by the backscatter off of the other horns. Gain comparisons between the 1- and 6-horn models in Fig. 11b show that there is a nonnegligible difference in gain. The 6-horn model shows less gain than the 1-horn model. The difference is associated with antenna and structural mode scattering effects that produce constructive and destructive interference.⁶ The horn mounting hardware are not included in the model so that the measurements include scattering effects from the horn assembly that are not in the model results. The full 6-horn FEKO model with one plane of symmetry requires 33 GB of RAM and 1692 s per frequency of computational time for a single precision simulation.

One way to reduce these computational requirements is to use MLFMM, which is an approximate technique to solve Maxwell's equations for electrically large problems. MLFMM is advantageous in that the efficiency increases with increasing electrical size of the problem space. However, due to being an approximate solution to Maxwell's equations, MLFMM does not necessarily enforce the reciprocity inherent in the equations. With this method, the full 6-horn model requires only 5.8 GB of RAM and about 936 s per frequency on a 12-core CPU. Alternatively MLFMM can be used on the GPU (NVIDIA Quadro K6000) and requires 3.2 GB of RAM and about 720 s per frequency. The numbers stated prove that MLFMM greatly reduces both the computational time and resources for simulating the 6-horn problem compared to without MLFMM and one plane of symmetry. However, MLFMM does not accurately predict nearest neighbor coupling or the cross-polarized radiation pattern. Spurious calculated data points predicted by MLFMM give false insight into the scattering produced by the other 5 terminated horns. Therefore, although MLFMM can, in general, greatly speed up simulation time over the full wave method, care must be taken when interpreting the fast method results.

In this case, it is better to accept a longer simulation time with fewer frequencies by using the full wave method than to use the fast method that naturally produces discrepancies that may or may not lead to confusion. With that said, FEKO does have the capability to solve surfaces with the combined field integral equation (CFIE) instead of the electric-field integral equation (EFIE). The CFIE combines the EFIE with the magnetic-field integral equation to potentially improve accuracy, but can only be applied to closed surfaces. Implementing CFIE could not be tested,

however, as the horn model is not a closed surface. Simulated results shown after Fig. 11b are produced without MLFMM.

There are pattern perturbations for the multiple horn arrangement owing to scattering effects that cause ripples in the TX (or RX) pattern. These effects are small in the forward direction for the 3 triangularly arranged horns but can be larger in the back lobes of the E-plane patterns where the horns are located. An example is shown in Fig. 12a at 12 GHz for a single horn in free space compared to the triangular arrangement of 3 horns. When the TX (top) horn is rotated 90° the E-plane pattern is similar to a single horn, indicating that scattering effects are larger with all horns co-polarized. With 6 horns, the perturbations are somewhat larger as shown in Fig. 12b where there is also more ripple in the forward direction with all 6 horns caused by scattering off of the other 3 horns. As mentioned previously, symmetry was not used because of the induced perfect cross-polarization of the transmit horn as seen in Fig. 12c. Here, symmetry produces an unrealistic result where there is complete cancellation of the cross-polarized fields from the transmitter, thereby reducing the cross-polarized patterns to numerical noise. Without symmetry, the model is still idealized, being most obvious in the cross-polarized component of the E-plane pattern. Shown in Fig. 12d, there is a deep null at boresight produced by the idealized model. This null is significantly deeper than what would be measured in practice and would predict a much larger cross-polarized isolation than what would be measured. Rotating the horn (or pattern) by 1° fills in the artificial null on boresight. Therefore, in cases such as this, introducing some small error in the model (e.g., rotation alignment error) is recommended to improve prediction accuracy for the actual horn configurations.

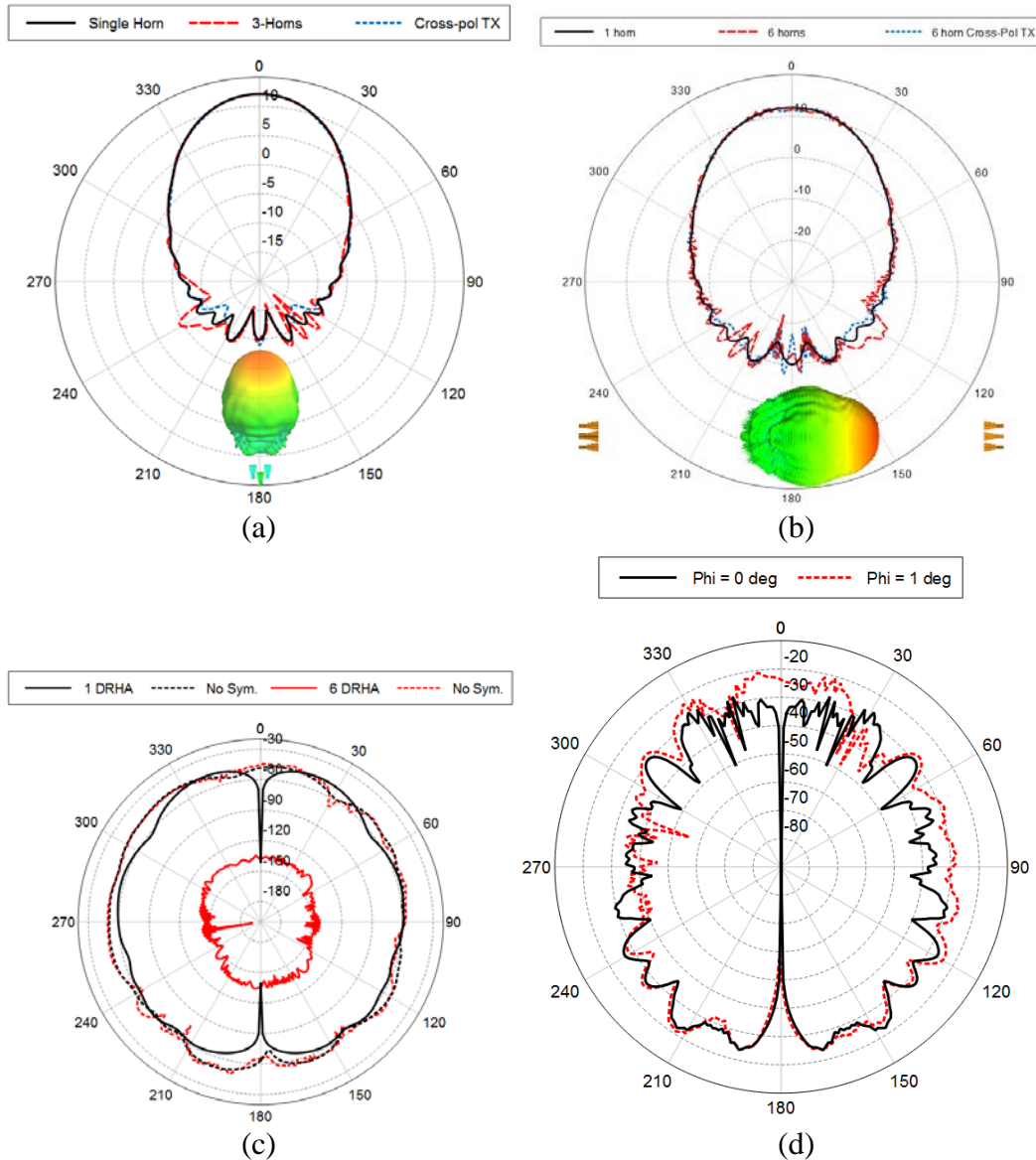


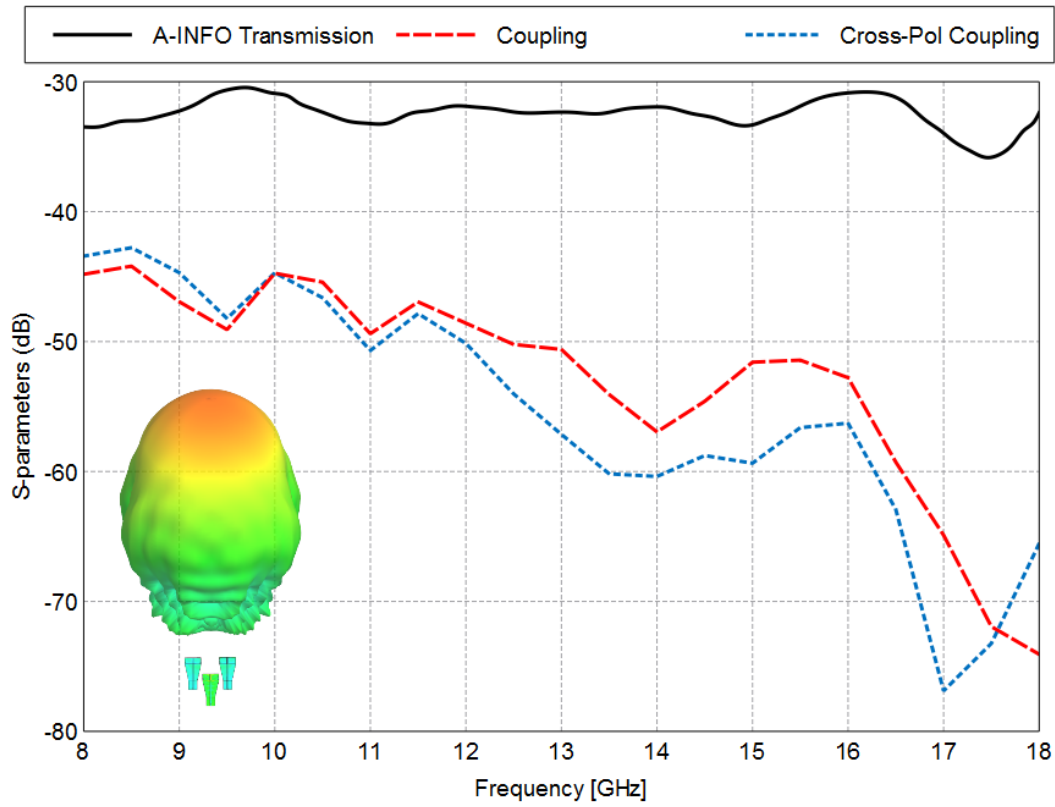
Fig. 12 The free space realized gain E-plane pattern at 12 GHz for DRHAs a) using the FEKO single-horn model compared to 3 horns, b) a single horn compared to the 6-horn model, c) the corresponding cross-polarized component with and without symmetry, and d) the rotated TX horn cross-polarized pattern

For a pair of matched horns in free space having gain, G_t and G_r , the calculated PL is almost exact compared to the FEKO result. But, a numerical model allows an estimate of horn-to-horn coupling and scattering effects from the horns' geometric arrangement. Such effects will cause deviations from the PL expected for a matched pair of TX and RX horns. The PL between 2 antennas separated by 2 m between apertures can be readily calculated according to the Friis equation. This loss includes the antenna gain (in dB) and is typically taken to be positive, often written as

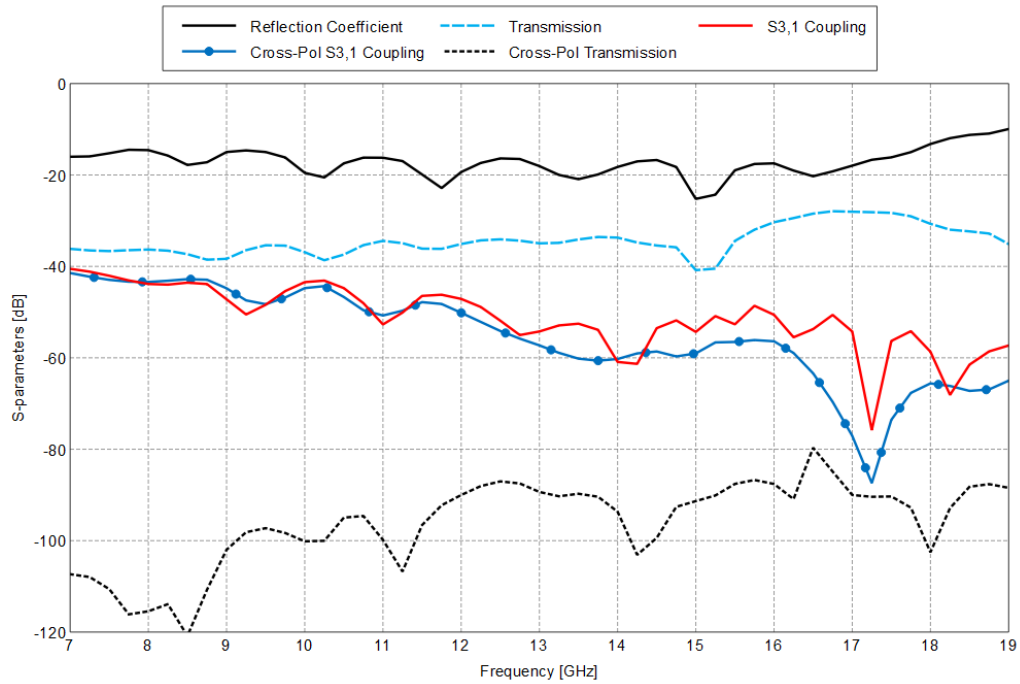
$$PL(dB) = 32.4 + 20\log[d(km)] + 20\log[f(MHz)] - G_t - G_r, \quad (1)$$

where $d(km)$ is the distance in kilometers and $f(MHz)$ is the frequency in megahertz. Given the A-INFO horn gain and assuming identical antennas the PL over 2 m can be calculated by Eq. 1, referred to as the A-INFO transmission. The simulated S-parameters for a 3- and 6-horn model are shown in Fig. 13a and b, respectively. The calculated transmission (or A-INFO calculated PL from Eq. 1) for a 2-m separation is shown in Fig. 13a. Also included are the simulation results for the coupling with a cross-polarized transmitter where the coupling (or cross-talk) to the nearby horns (S3, 1) at low frequency is roughly independent of the TX horn polarization. These S-parameters are somewhat different for the 6-horn model, indicating that all horns should be included to have the most accurate numerical model for the A-INFO horns as installed. The dip in transmission and S1, 1 near 15.5 GHz, are inherent to the horn model where there are corresponding dips in the boresight gain and S1, 1 for a single horn. The addition of the other 5 horns lowers the received power on boresight due to the slightly lower boresight gain induced by the pattern ripple. The S1, 1, coupling, and cross-polarized transmission all have more ripple due interference when including all 6 horns, which would not be seen with only 3 or 4 horns.

In the symmetric 3-horn arrangement, the cross-talk to the bottom 2 horns with the top horn transmitting is nearly identical. Also when the TX horn is rotated 90° the cross-talk is similar as shown in Fig. 13a. The cross-polarized transmission is lower than the co-polarized transmission by about 70 dB, which is 35 dB more than what would be expected for a typical horn. This is the result of the null on boresight in the cross-polarized pattern of an idealized model. By slightly rotating the transmitter one tenth of a degree, the difference is about 60 dB instead of 70 dB. In fact, an even smaller rotation of one millionth of a degree is enough to change the cross-polarized transmission result by as much as 5 dB. The cross-polarized coupling, on the other hand, is not much different than the co-polarized coupling in the 6-horn model as shown in Fig. 13 b. This implies that the coupling to nearest neighbor horns is roughly independent of polarization so it is dominated by antenna structural mode scattering. That is, the coupling to nearby horns is not direct coupling through the aperture but rather due to induced current on the horn by scattering from the TX horn sidelobes.



(a)



(b)

Fig. 13 The simulated S-parameters for ridge horn antennas for a) a 3-horn model and b) a 6-horn model

Using a single standard gain horn (SGH) antenna gain versus frequency in free space from FEKO, the PL (negative) is calculated for comparison to the FEKO transmission (S_{21}) result for matched antennas at a 2-m separation. There is a discrepancy at 12 GHz as shown in Fig. 14, but otherwise the difference is less than 0.3 dB. The difference is the scattering effect of the RX antenna. Similarly, the manufacturer's measured gain of the installed antennas can be used in Eq. 1 to estimate the PL neglecting scattering effects. With 6 horns, this scattering and the effect of the absorber-lined chamber will cause the laboratory setup to be slightly different than free space conditions. These differences are included in the measured S-parameters of the installed antennas, which represent the calibration of the empty chamber. Each TX/RX pair could have a slightly different frequency response that represents deviations from free space propagation. However, measurements indicate the horns have nearly identical gain versus frequency, so that deviations from free space conditions (and the FEKO model) are associated with scattering effects of the chamber and mounting hardware along with the combination of the DRHA and structural mode scattering.

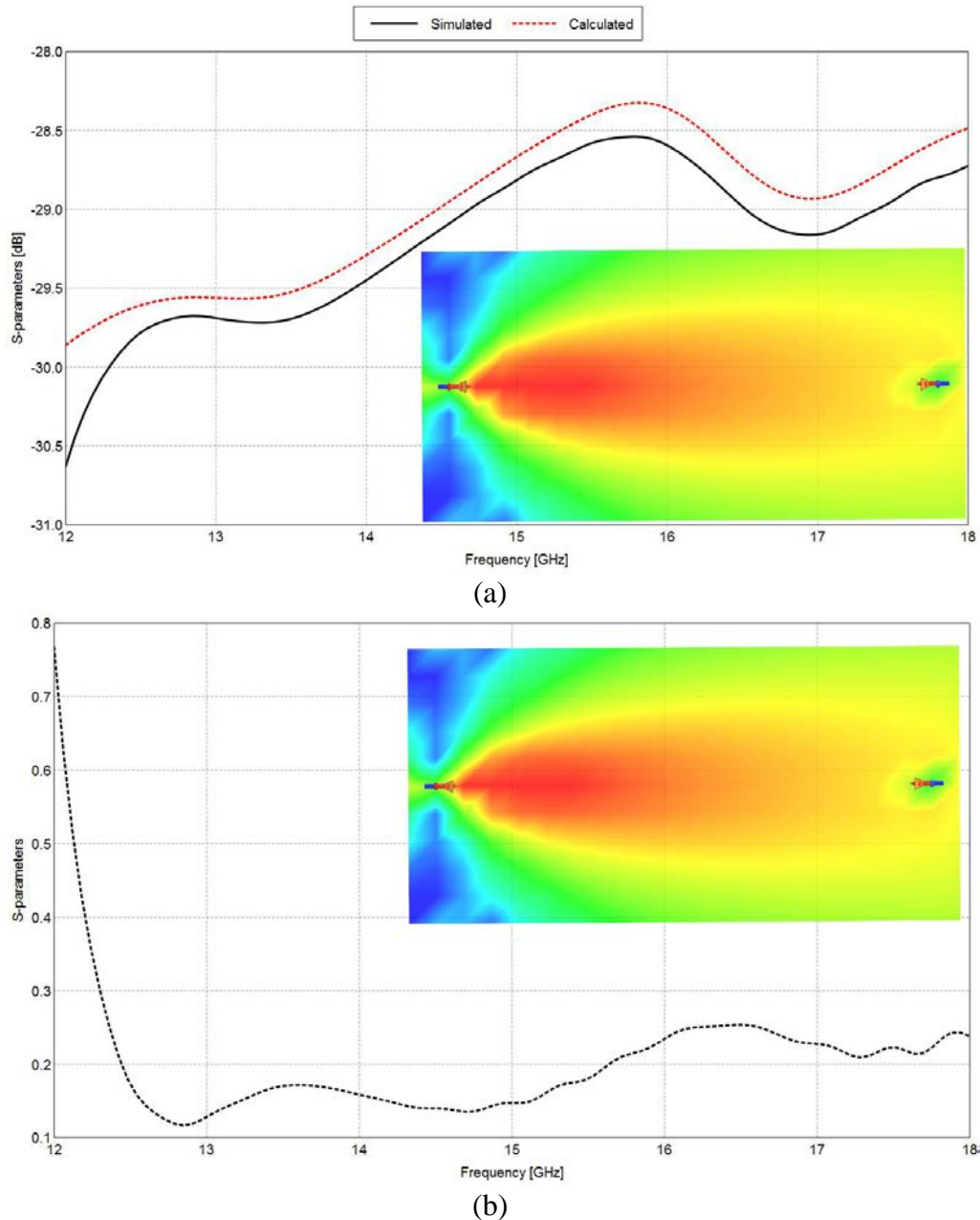


Fig. 14 The free space PL for SGH antennas a) from FEKO compared to the calculated PL and b) the difference vs. frequency

The manufacturer's measured gain of the A-INFO antenna 101 is used in Eq. 1 to estimate the PL (positive) over 2 m in free space neglecting scattering effects. The result is shown in Fig. 15 compared to the FEKO DRHA model. In this manner, the frequency-dependent gain can be included rather than a constant gain to estimate the frequency-dependent PL. Using the typical 10-dBi gain for the A-INFO horn does not capture this variation. However, there are significant differences in the A-INFO horn and the FEKO ridged horn model above 15 GHz, and this invalidates

some of the results that could be obtained with the FEKO model compared to measurements in the actual RF section at high frequency.

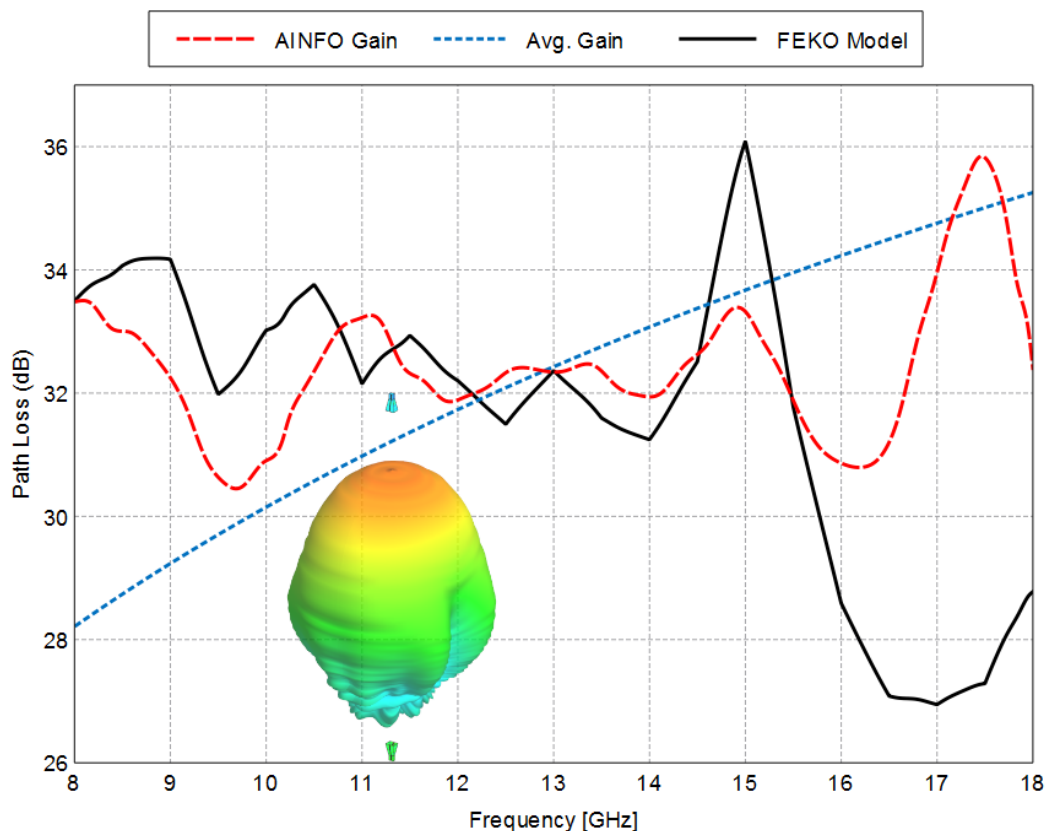


Fig. 15 The free space PL for 2 DRHAs from theory using the measured gain vs. frequency, the typical gain, and from a FEKO simulation

5. RF Section Measurements

The various horns are numbered as shown in Fig. 8b, where horns 4–6 are at the opposite end of the chamber. Thus, horn 1 and 4 are at the top where the triangular horn arrangements are geometrically aligned with respect to the center of each end wall. The measured $S(1,1)$ for horn 1 is shown in Fig. 16 compared to the single- and 6-horn FEKO models. The noise in this measurement is associated with the short section of cable connecting each horn to its chamber input not being included in the chamber calibration. The insertion loss is measured and used to correct the data, but the phase variation of the interconnect cables is part of the measurement. It could be suppressed by using fewer frequency samples (or averaging), but it is important that this noise is known to be part of the measured data. The $S(1,1)$ data for each horn are shown in Fig. 17. All the horns are similarly matched, but notice that horns 4–6 have a slight difference with increasing frequency.

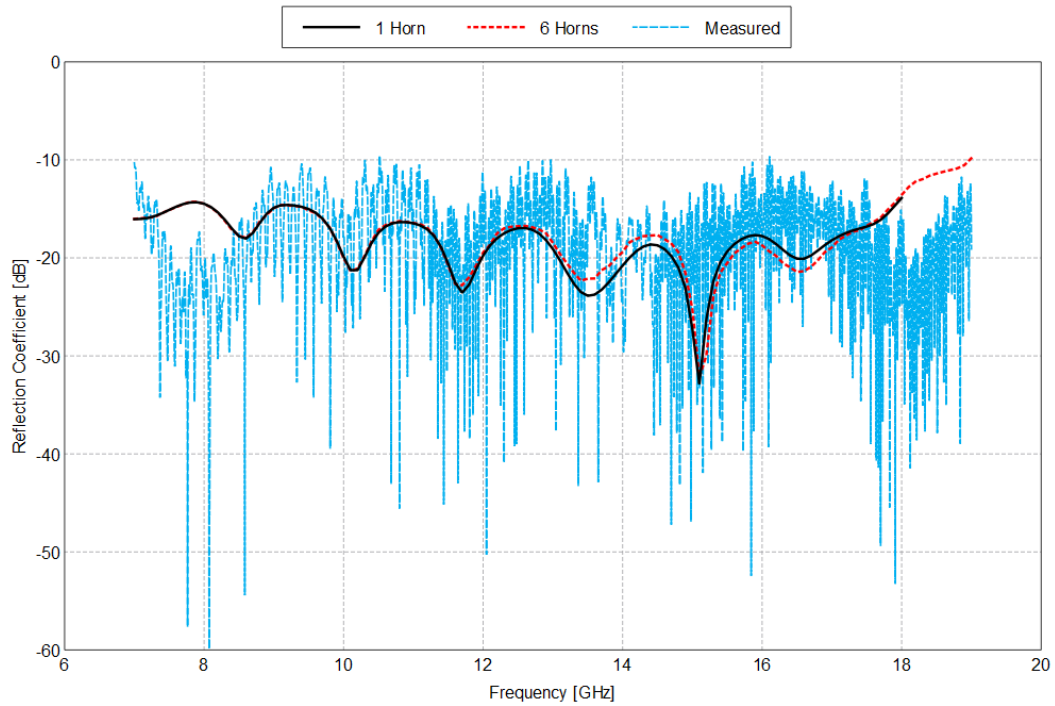


Fig. 16 The measured horn 1 reflection coefficient vs. frequency compared to the FEKO models

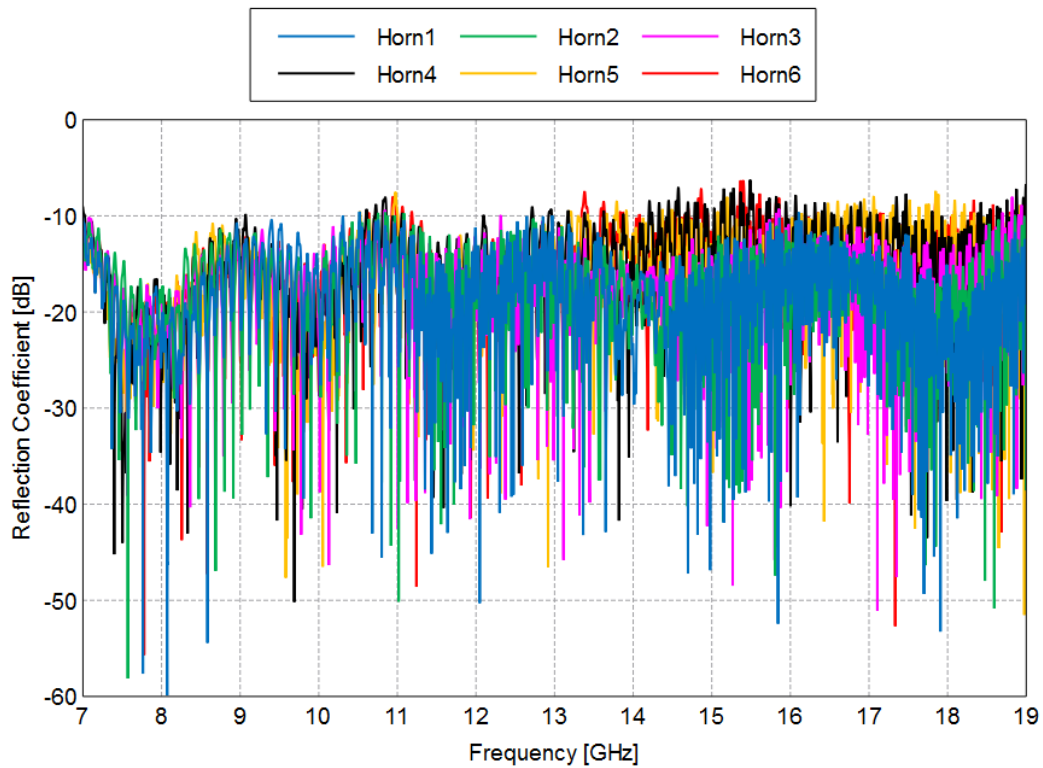


Fig. 17 The measured horn reflection coefficients vs. frequency

Since each horn has an equal length of cable not included in the VNA calibration, any measure of transmission or coupling will include the insertion loss of these cables. All these cable have almost identical insertion loss (positive) versus frequency and so are assumed to be the same with the measurement shown in Fig. 18. Thus, the measured transmission and coupling data are corrected by twice the interconnect cable insertion loss. This correction is used to avoid overestimating the actual transmission and coupling owing to only the horns and chamber. In practice, fewer frequency samples may be used to decrease the sweep time, which would under sample the interconnect cable variations with frequency and result in data that appear to have lower noise. For the purposes of this calibration report, the data are finely sampled to show that the noise cannot be removed without including the interconnect cables in the VNA calibration.

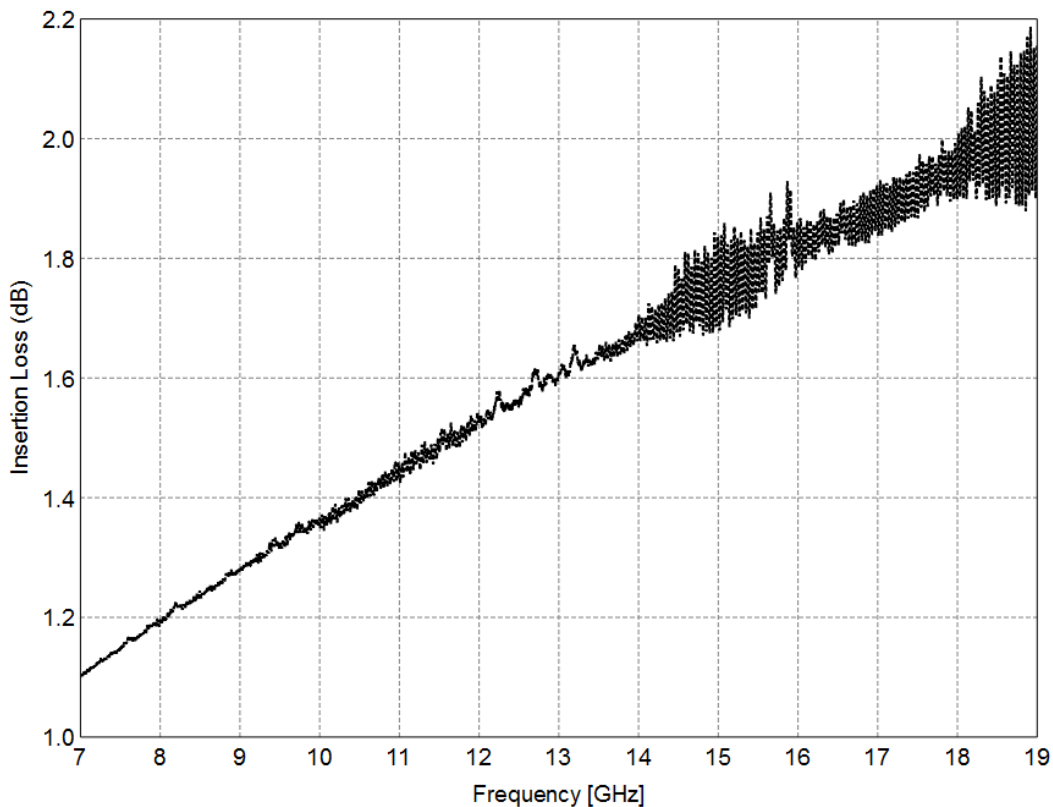


Fig. 18 The measured insertion loss for a short cable penetrating the CLL for connecting the horns

Horn 4 transmitting the measured coupling to the nearest neighbor horns is shown in Fig. 19 compared to the simulation result. The data are corrected by adding twice the cable insertion loss shown in Fig. 18 to the measurement. The results indicate the cross-talk to nearby horns is nearly identical. The FEKO model results are identical due to symmetry and similar to but somewhat larger than the measured

data. Thus, the FEKO 6-DRHA model in free space is useful for studying RF propagation in this chamber, but it does not exactly represent the RF section with the horns as-installed. The measured cross-talk compared to the VNA noise level is shown in Fig. 20. The noise level is that of the VNA using 100-Hz IF bandwidth, but the actual noise level for received power measurements can be limited by cross-talk. Thus, with a single horn transmitting, the minimum signal that can be received by nearby horns is determined by the horn-to-horn coupling. In the 8–18 GHz range, the VNA noise floor is 30–50 dB below the horn-to-horn cross-talk.

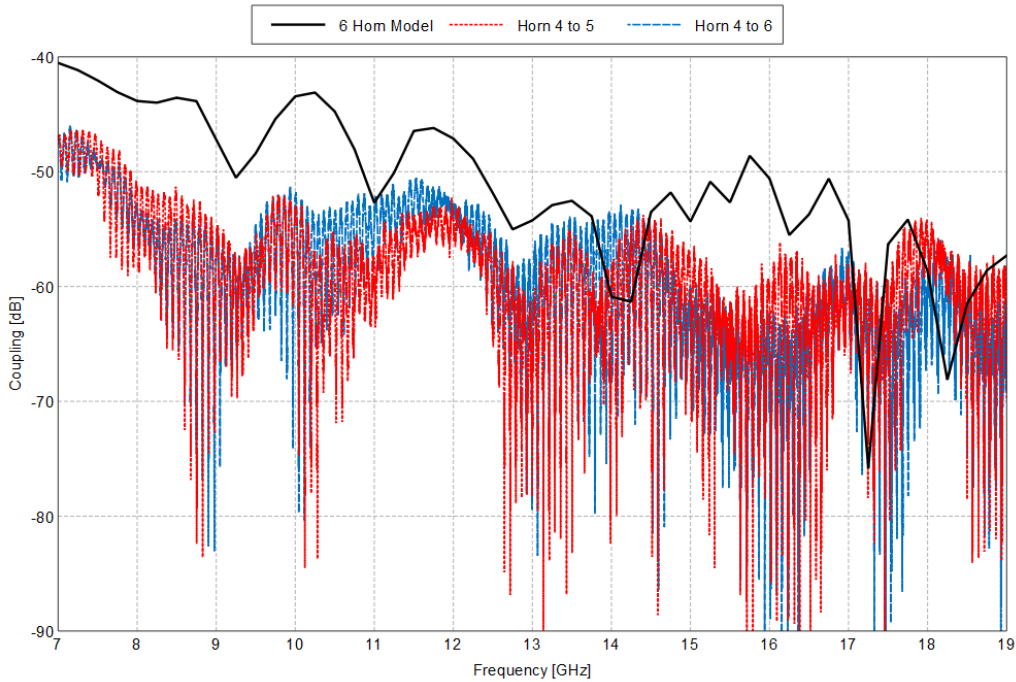


Fig. 19 The measured co-polarized horn coupling vs. frequency compared to the FEKO model

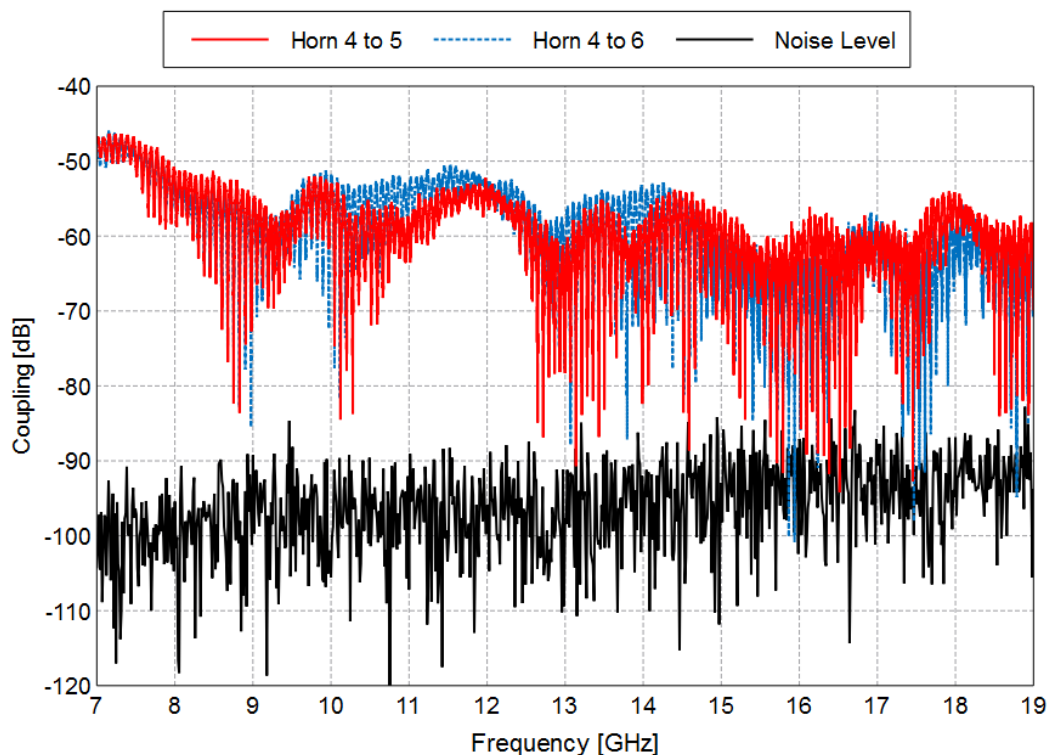


Fig. 20 The measured co-polarized horn coupling vs. frequency compared to the VNA noise level

The co-polarized transmission measurement is shown in Fig. 21 where aligned horns refers to geometrically aligned horns on each end of the chamber. With the top horn transmitting, the received signal of the bottom horns is slightly different indicating that the horns are not perfectly identical or the arrangement is not completely symmetric. The measurement has not been corrected for the interconnecting cable losses, so represents the PL from the chamber input not the horn input. Actual calibration of the RF section requires the PL from the horn apertures so that it includes only the free space PL plus scattering effects of the chamber and horns as constructed. The corrected data using the measured interconnecting cable insertion loss are shown in Fig. 22 indicating the frequency-dependent transmission (or PL) of the chamber as constructed.

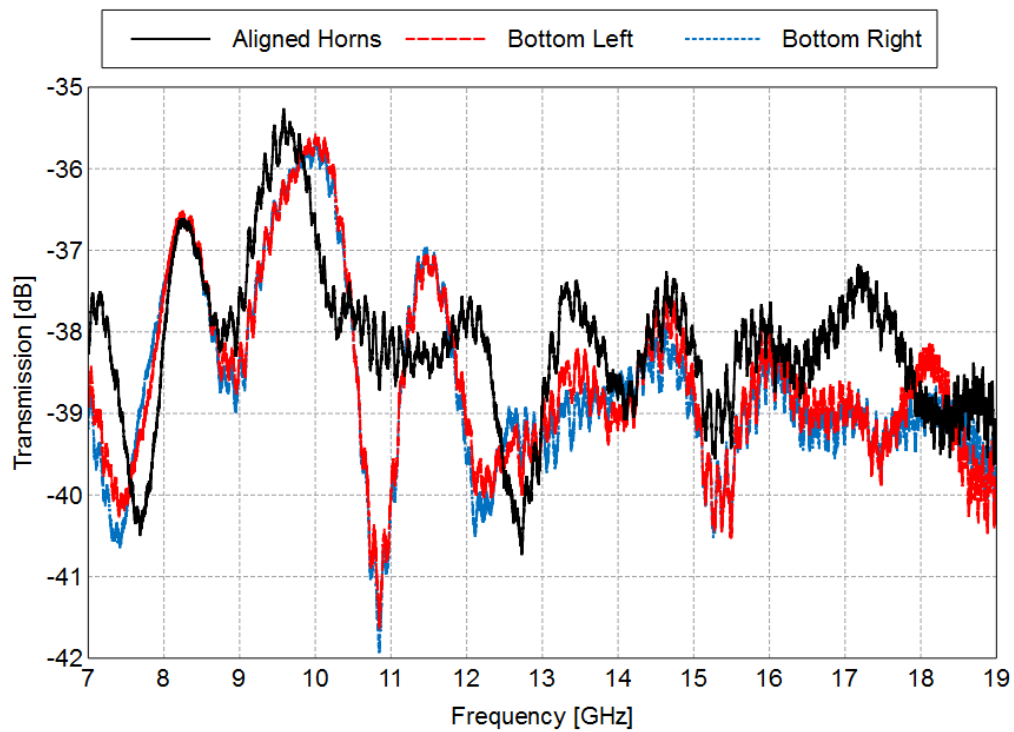


Fig. 21 The measured transmission for co-polarized horns vs. frequency without correction

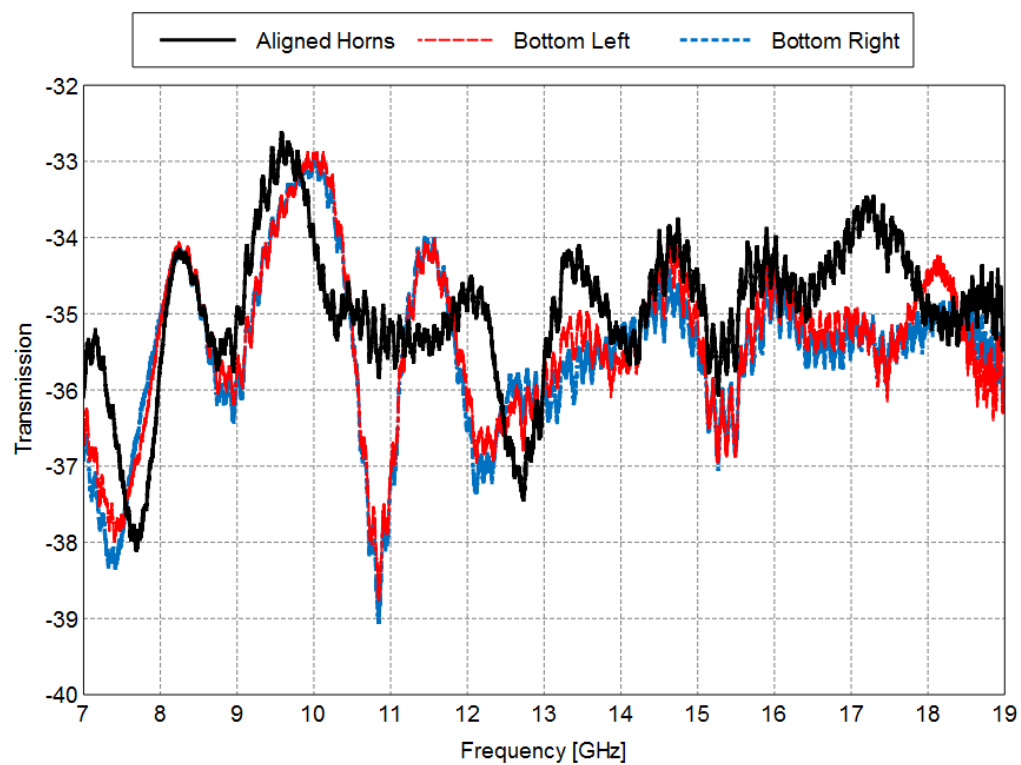


Fig. 22 The corrected data for transmission of co-polarized aligned horns vs. frequency

By rotating the top TX horn 90° the cross-polarized transmission and coupling to nearby horns can be measured as shown in Fig. 23. The coupling for a cross-polarized TX horn is similar to that for co-polarization at low frequency. This implies that coupling to nearby horns is dominated by structural scattering in the horn arrangement from the sidelobes of the TX horn. The transmission is as expected being about 35 dB below that measured for a co-polarized transmitter. At lower frequencies, the transmission between geometrically aligned horns is similar to when the horns are not aligned, as might be expected from the close geometry. The transmission to one of the not aligned horns has deep dropouts at some frequencies compared to the aligned (but cross-polarized) horns.

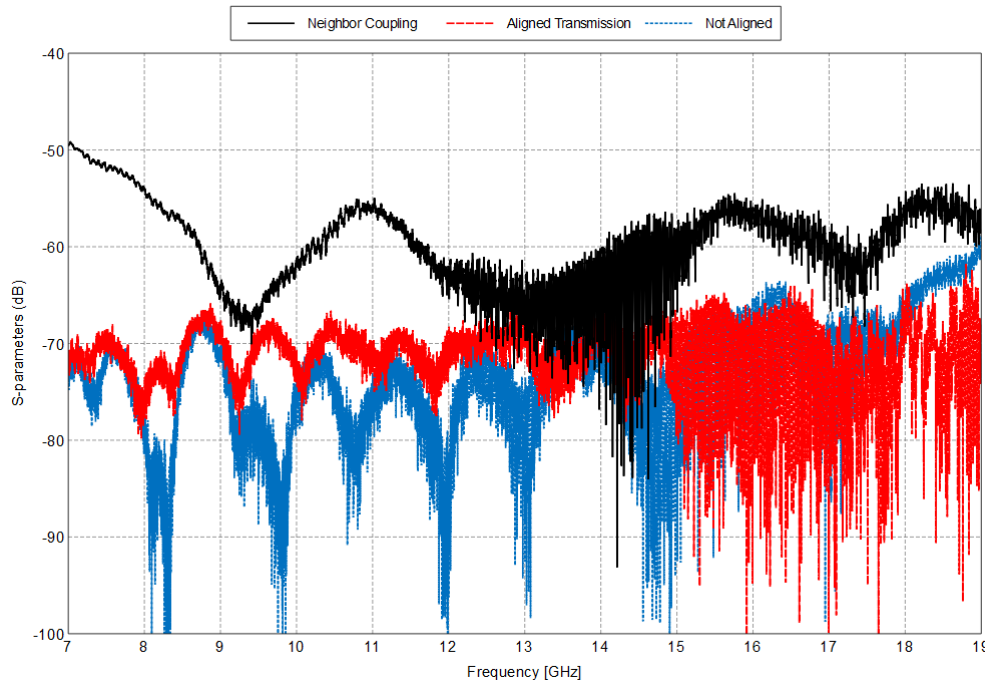
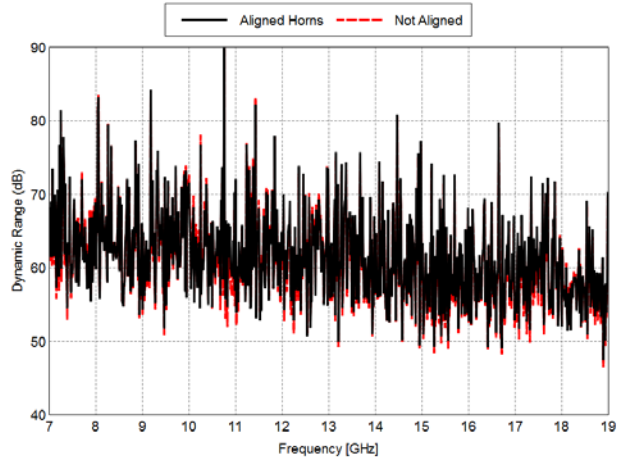
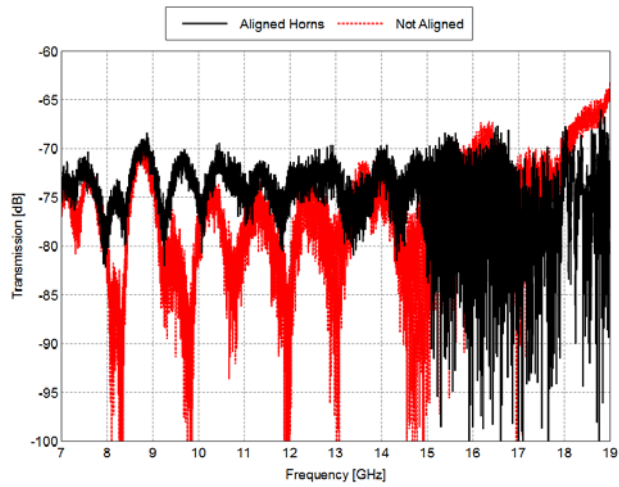


Fig. 23 The corrected data for transmission and coupling of a cross-polarized TX horn vs. frequency

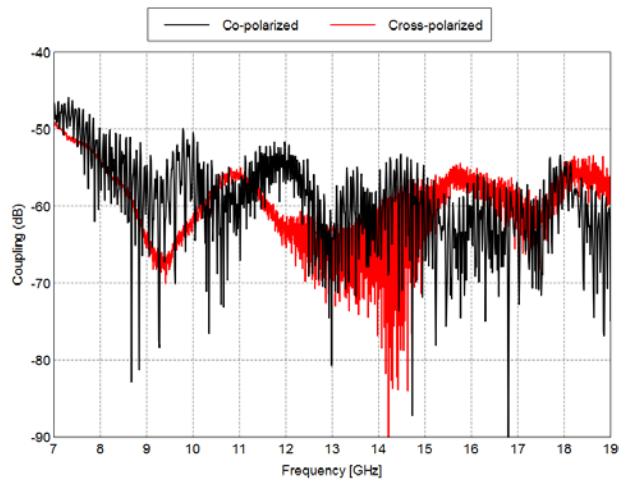
A summary of the measured transmission and coupling levels is shown in Fig. 24. In all cases, the measured data are corrected for twice the cable loss shown in Fig. 18. For co-polarized horns, the dynamic range for transmission is limited by the VNA noise level being about 60 dB over the frequency range as shown in Fig. 24a. For a cross-polarized TX horn, the transmission is lower by the RX horn cross-polarization isolation so that the available dynamic range above the VNA noise level is limited as shown in Fig. 24b. With a cross-polarized TX horn, the transmission to the nonaligned horn can be larger or smaller than that to the aligned horn depending on frequency. For a nearby horn in reception, the noise level is established by the coupling from the TX horn. The measured coupling is shown in Fig. 24c for both a co- and cross-polarized TX horn, indicating that this coupling to nearest neighbor horns is roughly independent of polarization.



(a)



(b)



(c)

Fig. 24 The measurement summary for a) the dynamic range for co-polarized transmission based on noise level, b) the cross-polarized transmission and noise level, and c) the noise level for reception based on nearest neighbor coupling

A summary of the measured co-polarized transmission for aligned horns is shown in Fig. 25 compared to the calculated PL using the A-INFO horn gain and simulated with the FEKO 6-horn model in free space. The data in this figure have not been corrected for the additional cable insertion loss. The corrected data are shown in Fig. 26 so they are larger by twice the cable loss of Fig. 18. The calculated PL for a pair of co-polarized and aligned A-INFO horns is also corrected to correspond to the reduced gain in a 6-horn arrangement (see Fig. 11b). The FEKO model showed that the gain of a single horn when configured in the 6-horn arrangement is lower at most frequencies compared to an isolated horn gain. So twice the correction factor in Fig. 11b is applied to the PL calculated with a pair of A-INFO horns. The FEKO DRHA model is similar but not identical to the actual horn, but the numerical model indicates that the boresight gain would be reduced. So the difference between a single DRHA and the 6-horn configuration in FEKO is applied to the A-INFO horn gain used in the PL calculated by Eq. 1. The corrected results are shown in Fig. 26 where the calculated transmission from Eq. 1 or from the 6-horn FEKO model are within about 2 dB of the measured data. The difference is associated with additional scattering effects of the chamber not captured in the free space calculation or simulation. This is probably additional scattering effects of the horn mounting hardware and the gap in the absorber around the mounting head as installed (see Fig. 7a).

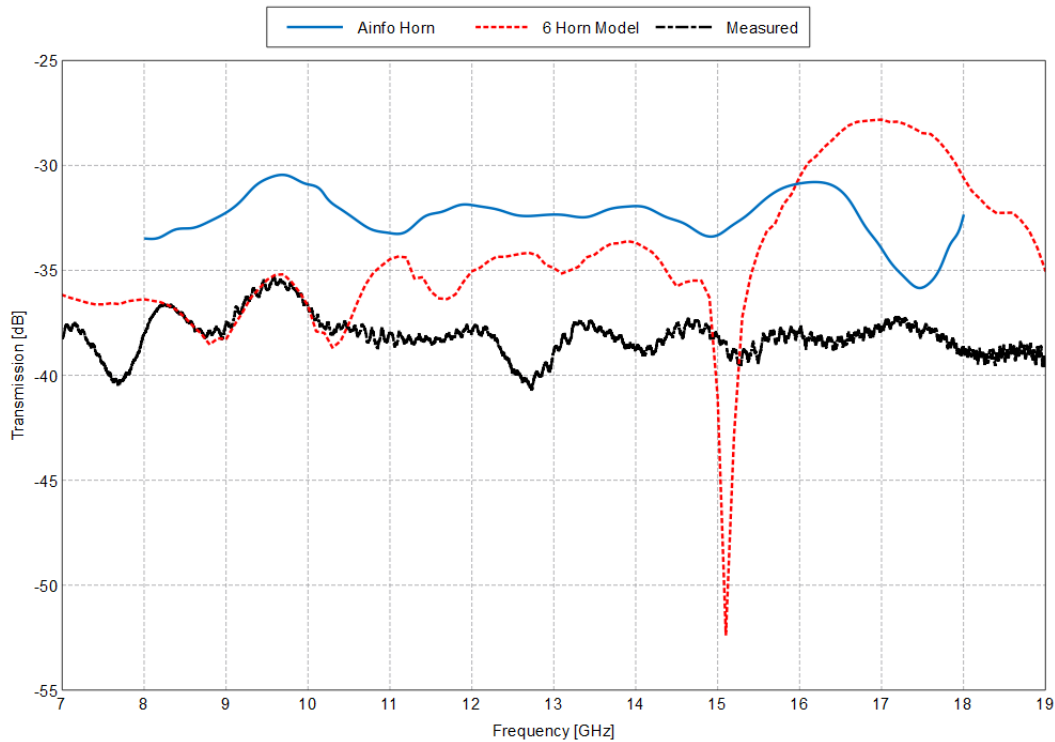


Fig. 25 The measured data without correction for transmission of co-polarized horns compared to calculated and simulated PL

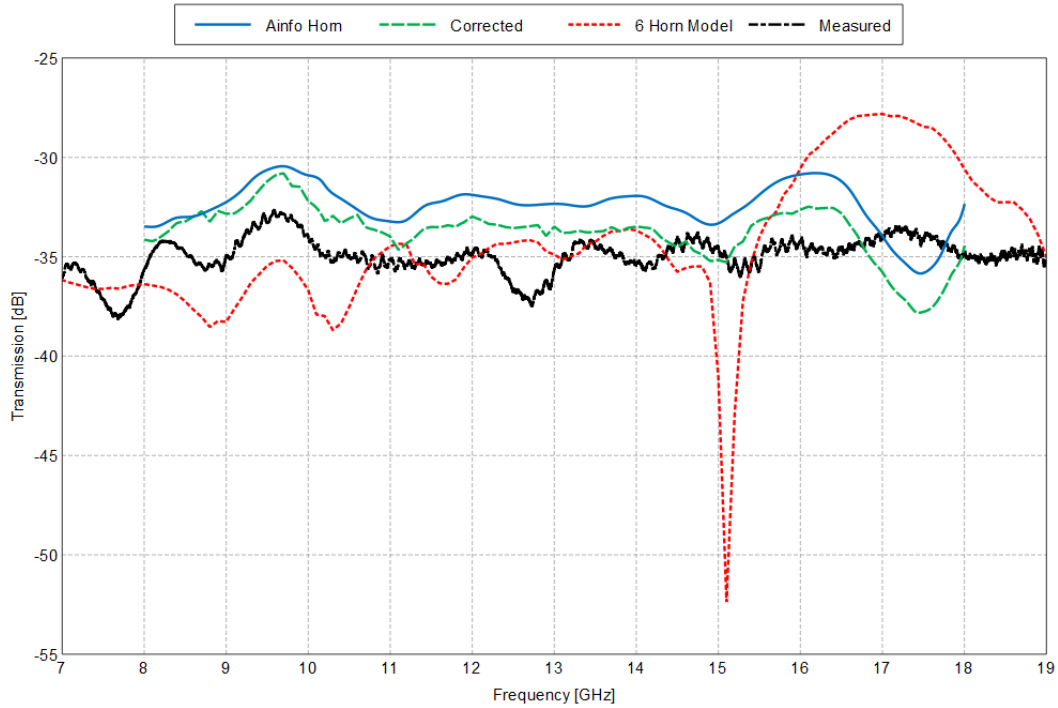


Fig. 26 The corrected data for transmission of co-polarized horns vs. frequency

The comparison between the measured and calculated or simulated S-parameters is summarized in Fig. 27 for co-polarized horns. The measured reflection coefficient is similar to the FEKO model but includes noise associated with the interconnecting cables and connectors that are not included in the VNA calibration. The measured transmission is similar to that calculated for the A-INFO corrected horn gain using Eq. 1. The measured coupling to a nearby RX horn is similar to the FEKO model except at low frequency where the simulated coupling results are a few decibels larger. The measured noise level is also shown, which can limit the available dynamic range depending on the type of experiments conducted in the RF chamber.

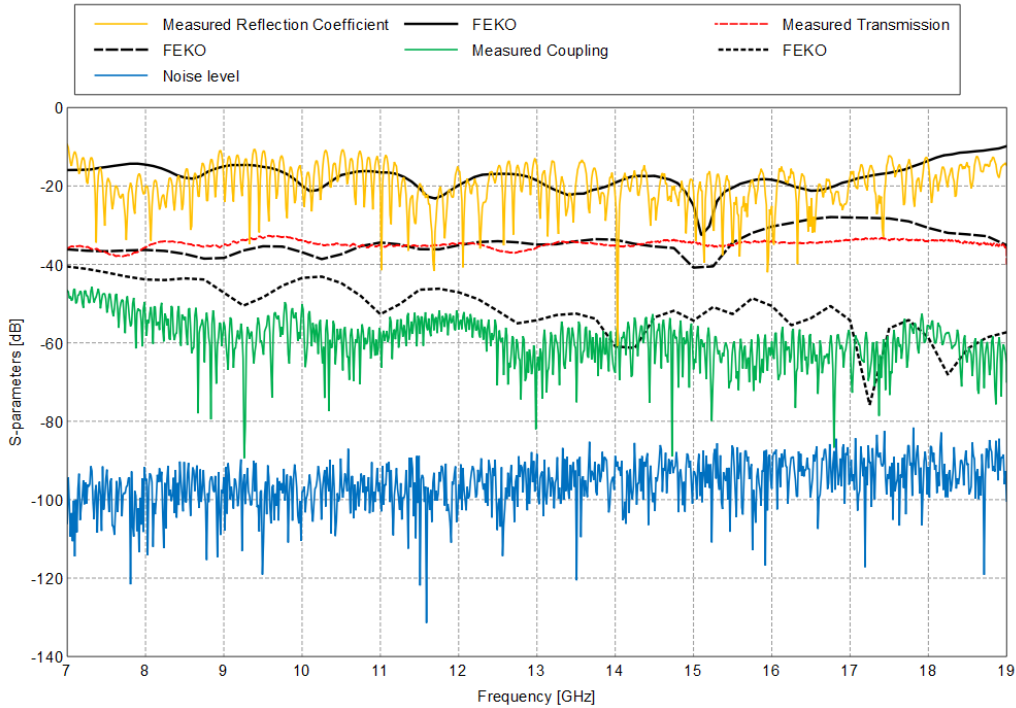
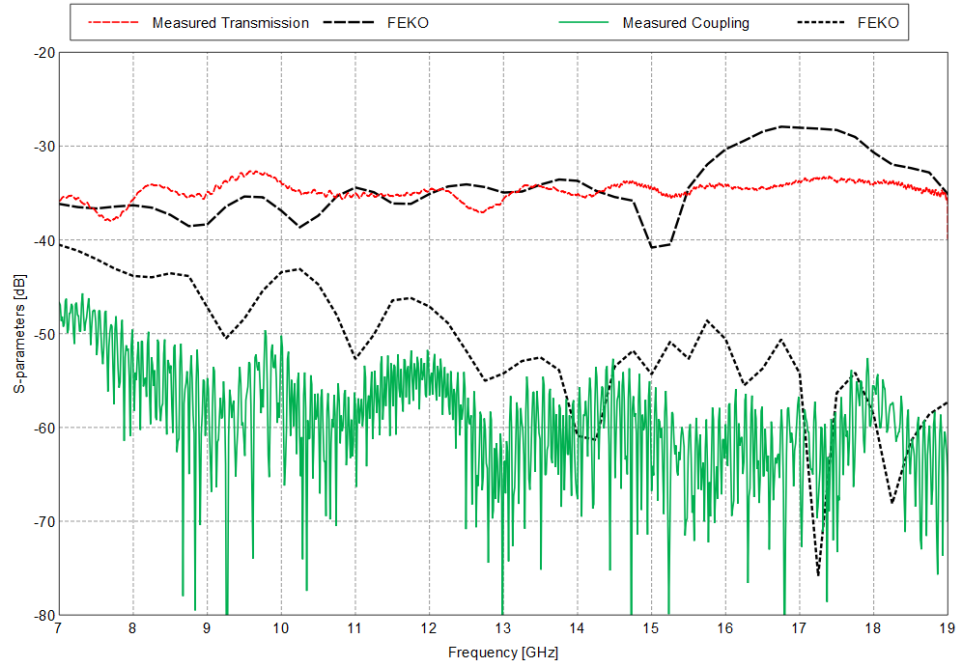


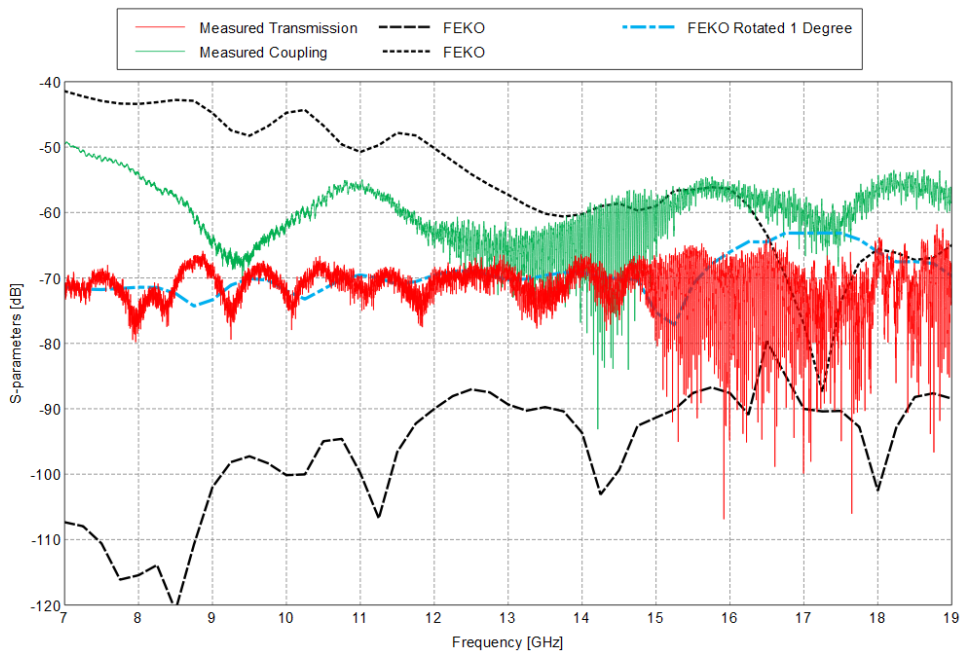
Fig. 27 The corrected co-polarized data summary compared to calculated/simulated results vs. frequency

The corrected data and FEKO simulated results for co-polarized transmission and coupling are shown in Fig. 28a on an expanded scale. The transmission between geometrically aligned horns for the FEKO 6-horn model is within about 2 dB of the measurement below 15 GHz. These small differences are the influence of the horns as-installed in the absorber-lined chamber compared to the 6-horn arrangement in free space. At higher frequencies, there are large deviations associated with the difference between the FEKO DRHA model and the A-INFO horn gain (see Fig. 11a). For co-polarized coupling to the nearest neighbor horn, the FEKO model is in better agreement at higher frequency. At lower frequencies, the wavelength is on the order of the feature size of the horn mounting hardware and shaft assembly, which could lead to more destructive interference. The corrected data and FEKO simulated results for cross-polarized transmission and coupling are shown in Fig. 28b on an expanded scale. The agreement is not as good as for the co-polarized results primarily associated with the idealized model even without using symmetry. This can be seen by rotating the TX horn in the FEKO model by 1° , which produces results similar to the measured transmission. The measured coupling for both a co- and cross-polarized TX antenna is smaller than simulated but about the same level independent of polarization. The simulated results do not exactly reproduce measurements especially for a cross-polarized TX since the FEKO model is an idealized representation of the actual DRHA configuration. The results also have

differences associated with scattering effects of the horns as-installed in the absorber-lined chamber. Comparison to the measurements indicates that small errors can be introduced in the FEKO model to better represent the horn configuration in the RF propagation section.



(a)



(b)

Fig. 28 The corrected a) co-polarized and b) cross-polarized data summary compared to FEKO simulated results vs. frequency

6. Conclusions

All the cables/connectors used to connect the network analyzer to the RF propagation section are calibrated out of the measurements, except the short cables and connectors between the input to the chamber and the horn input. The insertion loss of these cables is measured separately and the data corrected for this additional loss. VNA calibration and measurements were conducted over frequencies of 7–19 GHz, where the measured transmission and coupling corrected data represent the calibration of the entire RF propagation section. Calculated PL and numerical simulations are shown to demonstrate that the chamber performance can be approximated by free space calculations or numerical simulations of an idealized horn configuration. These calculated or numerical results are not exact, since they do not include all the various scattering effects versus frequency owing to the horn mounting hardware and motor assembly. Nevertheless, the numerical model does approximately capture the influence of the 6-horn configuration and so can be useful for modeling the various experiments that can be conducted in the CLL propagation section. However, the FEKO model is idealized in that the horns are geometrically aligned and symmetric about the vertical centerline so that introducing small asymmetries can often better match the data, especially for cross-polarized measurements. In this manner, some expectation of the measured results can be obtained through simulation. In addition, a numerical model can be useful to estimate dynamic range and the influence of an arbitrary polarization mismatch. Although the measured data for the CLL propagation section with corrections represent its calibrated performance as-installed, the numerical model can also be useful for additional insight into the utility and limitations of experiments conducted in the CLL facility.

7. References

1. PXIe-1085. Austin (TX): National Instruments; 2016 [accessed 2016 Oct 17]. <http://sine.ni.com/nips/cds/view/p/lang/en/nid/210863>.
2. MAST Technologies homepage. San Diego (CA): MAST Technologies; 2016 [accessed 2016 Oct 17]. www.masttechnologies.com.
3. LB-80180. Chengdu (China): A-INFO Inc.; 2011 [accessed 2016 Oct 17]. http://www.ainfoinc.com/en/pro_pdf/new_products/antenna/Broadband%20Horn%20Antenna/tr_LB-80180.pdf.
4. Tesny N. Electronic warfare closed loop laboratory antenna motor software and hardware development. Adelphi (MD): Army Research Laboratory (US); 2106 Sep. Report No.: ARL-TN-0779.
5. FEKO. Troy (MI): Altair Engineering; 2015 [accessed 2016 Oct 17]. www.feko.info.
6. Balanis CA. Antenna theory analysis and design, 3rd ed. Hoboken (NJ): Wiley-Interscience; 2005.



INTENTIONALLY LEFT BLANK.

Appendix. Equipment Used

This Appendix summarizes the equipment used in the operation and testing of the Closed Loop Laboratory radio frequency (RF) section, along with the commercially available absorber and horn antennas used in constructing the RF section. The equipment list is shown in Table A-1. The calibration certificates for the electronic calibration (ECal) module and Peripheral Component Interconnect Extensions for Instrumentation Express (PXIe) vector network analyzer (VNA) are included in Figs. A-1 and A-2, respectfully. Both were calibrated by the manufacturer within the past year. The data sheet for the MAST Technologies broadband foam absorber is shown in Fig. A-3. Note that this material is no longer available from this manufacturer. The A-INFO horn typical gain and cross-polarized response are shown in Figs. A-4 and A-5, respectfully.

Table A-1 Equipment and parts list

1.	Keysight Technologies M9375A PXIe VNA, 300 kHz to 26.5 GHz
2.	Keysight Technologies N4691B ECal module, 300 kHz to 26.5 GHz, 3.5 mm, 2-port
3.	MegaPhase 10-ft SMA, male to male, coax cable P/N: EMC2-3131-120/1GVT4 16057901 002
4.	Crystek 2-ft SMA, male to male coax cable P/N: 1408-10, CCSMA-MM-LL142-24
5.	2 × SMA female to female adapters
6.	National Instruments (NI) PXIe-8135 controller
7.	NI PXI 1085 18-slot chassis

 KEYSIGHT TECHNOLOGIES	Keysight Technologies Malaysia Sdn Bhd (463532-M) Bayan Lepas Free Industrial Zone 11900 Penang, Malaysia.	 5962-0476

Certificate Of Calibration

Certificate No: N4691BSG5223005620160308
Manufacturer: Keysight Technologies
Model No: N4691B
Options Installed With Specifications: 00M

Description: 3.5mm ECAL MODULE
Serial No: SG52230056

Date of Calibration: 08-MAR-2016
Temperature: (23 ± 0.5) °C
Procedure: MTA-T0215, MTA-T0214

Humidity: (20 to 55) %RH

This certifies that the above product was calibrated in compliance with a quality system registered to ISO 9001:2008, using applicable Keysight Technologies' procedures.

As Received: Factory tested - No incoming data available.

As Shipped Conditions: At the completion of the calibration, measured values were IN-SPECIFICATION at the points tested.

These calibration procedures and test points are those recommended in a procedure developed by Keysight.

Remarks or special requirements:

Note 1: A Test Station consists of equipment with individual calibration due dates and/or local calibration.

Traceability Information: Traceability is to the International System of Units (SI), consensus standards or ratio type measurements through national standards realized and maintained by the NIST U.S., NRC Canada, NMJ Japan, KRISS Korea, Euramet members (NPL, PTB, etc.), NML-SIRIM in Malaysia or other National Measurement Institutes signatories to the CIPM MRA. Supporting documentation relative to traceability is available for review by appointment. This report shall not be reproduced, except in full, without prior written approval of the calibration facility.

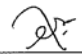
Calibration Equipment Used:

Model Number	Model Description
N5230A	PNA Network Analyzer
ET33700,004	3.5mm ET Calibration Kit
E8364C	PNA Network Analyzer
N5230A	PNA Network Analyzer

Date used: Date equipment used in this calibration.

Trace Number	Date Used	Cal Due Date
PC7688	08-Mar-2016	24-Apr-2016
PB7064	08-Mar-2016	15-Jun-2016
PC7712	08-Mar-2016	28-Aug-2016
PC7063	08-Mar-2016	18-Oct-2016

Print Date: 09-MAR-2016




 Tay Eng Su
 Quality Manager

Keysight Technologies			
DD	MM	YY	BY
CAL	08	03	16
DUE			

cert form rev h

Page 1 of 1

Fig. A-1 Electronic calibration module calibration certificate

	Keysight Technologies Malaysia Sdn Bhd (463532-M) Bayan Lepas Free Industrial Zone 11900 Penang, Malaysia	 <small>5162-0476</small>

Certificate of Calibration

Certificate No: 4166930-4988644-1

Manufacturer: Keysight Technologies
Model No: M9375A
Options Installed With Specifications: N/A

Description: 300KHz-26.5GHz PXIe Network Analyzer
Serial No: SG54321029

Date of Calibration: 11-NOV-2015

Temperature: (23 ± 3) °C

Humidity: (40 to 70)% RH

Procedure: EPSG1024199

This certifies that the above product was calibrated in compliance with a quality system registered to ISO 9001:2008, using applicable Keysight Technologies' procedures.

As Received: Factory tested. No incoming data available.

As Shipped Condition: At the completion of the calibration, measured values were IN SPECIFICATION at the points tested.

These calibration procedures and test points are those recommended in a procedure developed by Keysight.

Remarks or special requirements:

Traceability Information: Traceability is to the International System of Units (SI), consensus standards or ratio type measurements through national standards realized and maintained by the NIST U.S., NRC Canada, NMJ Japan, KRISS Korea, Euramet members (NPL, PTB, etc.), NML-SIRIM in Malaysia or other National Measurement Institutes signatories to the CIPM MRA. Supporting documentation relative to traceability is available for review by appointment. This report shall not be reproduced, except in full, without prior written approval of the calibration facility.

Calibration Equipment Used

Date Used: Date equipment used in this calibration

<u>Model Number</u>	<u>Model Description</u>	<u>Trace Number</u>	<u>Date Used</u>	<u>Cal Due Date</u>
N4691B	3.5mm Electronic Cal Kit	PB4202	11-NOV-2015	03-MAR-2016
N4691B	3.5mm Electronic Cal Kit	PB4191	11-NOV-2015	13-FEB-2016
N4691B	3.5mm Electronic Cal Kit	PB4190	11-NOV-2015	13-FEB-2016
N8488A	Average Power Sensor	PA4107	11-NOV-2015	02-APR-2016
N5245A	PNA-X NETWORK ANALYZER	PB4232	11-NOV-2015	27-JUN-2016
N1914A	EPM Series Power Meter	PB4201	11-NOV-2015	03-APR-2016

Print Date: 12-NOV-2015

cert form rev h



Tay Eng Su
Quality Manager

Page 1 of 1

Fig. A-2 Network analyzer calibration certificate

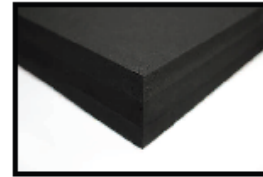


Broadband Multilayer Foam Absorber



MF51-0006-00

MAST Technologies' Multilayer Foam Absorber product series is a lightweight conductive carbon loaded sheet stock providing broadband reflection loss at microwave frequencies. Due to the tapered resistance of each layer in the multilayer stack, they exhibit high reflection loss and are intended to be applied to metal surfaces inside test boxes, housings, radomes, network enclosures, or antennae. Multilayer Foam Absorbers attenuate energy at normal and high angles of incidence at frequencies from 1 GHz to 18 GHz.



APPLICATIONS

RF Test Boxes/Fixtures
Antenna Pattern Performance
Sidelobe/backlobe reduction
Resonant Cavity Attenuation
EMI Reduction
Rx/Tx Antenna Isolation
Radar Cross Section Reduction

FEATURES & BENEFITS

Lightweight foam
Cost effective broadband material
Easily applied with PSA
Most broadband absorber material
RoHS Compliant
Halogen Free

TYPICAL PROPERTIES

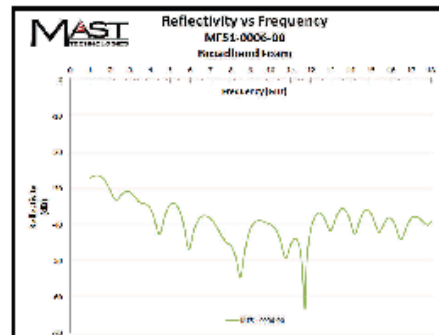
Thickness: 4.50" (114.3mm)
Adhesive Thickness: 0.005" (0.12mm)
Color: Black
Operating Temperature: -60°F to 250°F
Flammability Rating: Not Rated

PART NUMBERING: MF51-0006-00

XX = 00: No PSA backing
XX = 01: PSA backing
XX = >10: Die Cut

ELECTRICAL PERFORMANCE

This performance plot illustrates the reflectivity performance of this material. Reflectivity is measured in an NRL Arch, for more information on the NRL Arch test set-up, please refer to Tech Bulletin 101. Additional electrical test data may be available upon request.



METHOD OF APPLICATION

The primary method of application for Multilayer Foam Absorbers is utilizing a Pressure Sensitive Adhesive (PSA) backing. MAST proudly uses 3M transfer tapes on its Multilayer Foam Absorbers. Contact MAST technical representatives for a datasheet on the PSA.

Other liquid and paste adhesive may be recommended. Con-

AVAILABILITY

Standard Sheet Sizes: 24" x 24" (610 x 610mm)
Custom Sizes Available
Format: Sheets, Die Cut

MAST Technologies
6370 Nancy Ridge Dr.
Suite 103
San Diego, CA 92121
U.S.A.

tel+ 1.858.452.1700

www.masttechnologies.com

Revision: January 2012

All information on this data sheet is based on laboratory testing and is not intended for design purposes.
MAST Technologies makes no representations or warranties of any kind concerning this data.

Fig. A-3 Foam absorber data sheet¹

¹ MAST Technologies homepage. San Diego (CA): MAST Technologies; 2016 [accessed 2016 Oct 17].
www.masttechnologies.com.

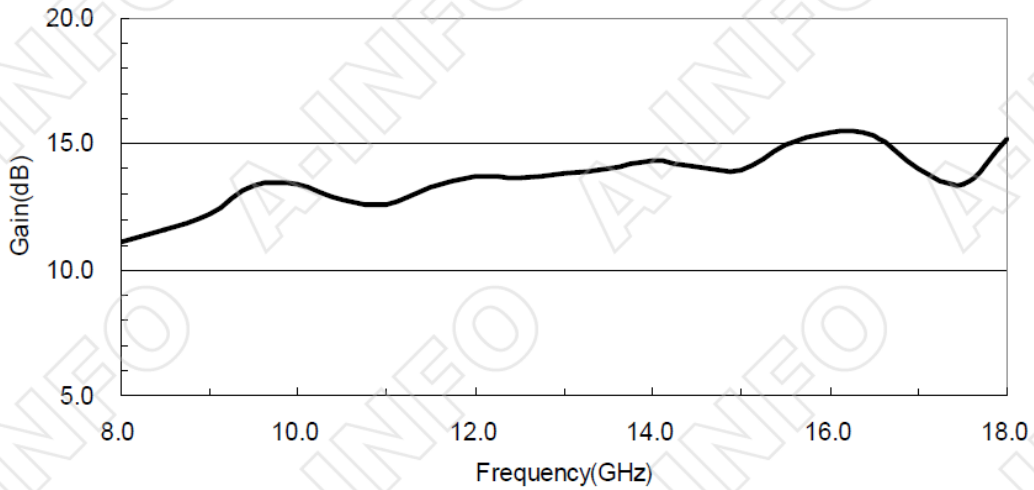


Fig. A-4 A-INFO horn typical gain vs. frequency (image courtesy of A-INFO²)

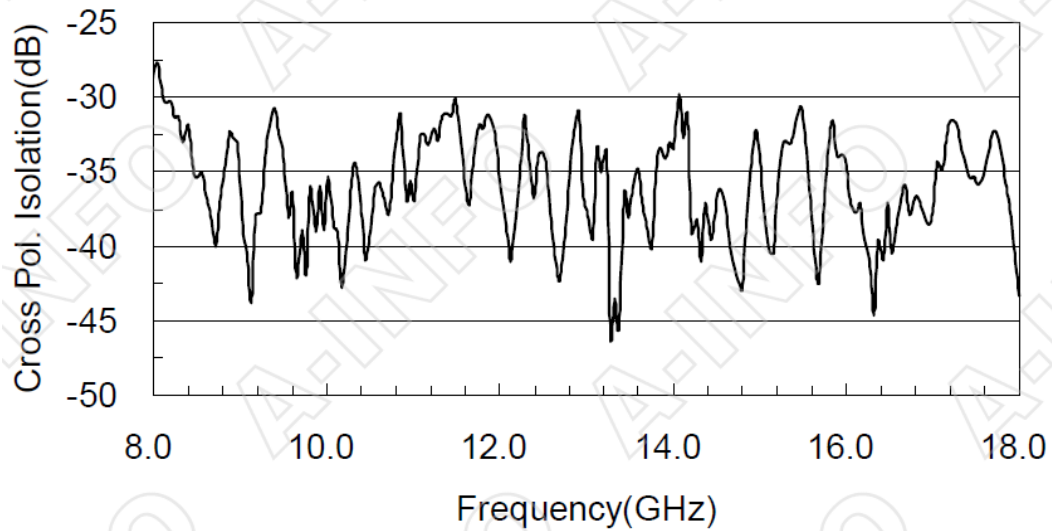


Fig. A-5 A-INFO horn typical cross-polarized response vs. frequency (image courtesy of A-INFO²)

² LB-80180. Chengdu (China): A-INFO Inc.; 2011 [accessed 2016 Oct 17]. http://www.ainfoinc.com/en/pro_pdf/new_products/antenna/Broadband%20Horn%20Antenna/tr_LB-80180.pdf.

List of Symbols, Abbreviations, and Acronyms

ARL	US Army Research Laboratory
CFIE	combined field integral equation
CLL	Closed Loop Laboratory
CPU	central processing unit
DRHA	dual-ridged horn antenna
ECal	Electronic Calibration
EFIE	electric-field integral equation
E-field	electric-field
GPU	graphics processing unit
IF	intermodulation frequency
MLFMM	multi-level fast multipole method
NI	National Instruments
PL	path loss
PXle	Peripheral Component Interconnect Extensions for Instrumentation Express
RAM	random-access memory
RCS	radar cross section
RF	radio frequency
RX	receive
SGH	standard gain horn
TX	transmit
USB	universal serial bus
VNA	vector network analyzer

1 DEFENSE TECHNICAL
(PDF) INFORMATION CTR
DTIC OCA

2 DIRECTOR
(PDF) US ARMY RESEARCH LAB
RDRL CIO L
IMAL HRA MAIL & RECORDS
MGMT

1 GOVT PRINTG OFC
(PDF) A MALHOTRA

4 DIRECTOR
(PDF) US ARMY RESEARCH LAB
RDRL SER M
WILLIAM COBURN
SETH A MCCORMICK
CHARLES DIETLIEN
RDRL SER U
MATHEW HIGGINS